Published in final edited form as:
Acta Biomater. 2021 January 15; 120: 277–292. doi:10.1016/j.actbio.2020.06.027.

Crystal nucleation and growth of spherulites demonstrated by coral skeletons and phase-field simulations

Chang-Yu Sun[1,2], **László Gránásy**[3], **Cayla A. Stifler**[1], **Tal Zaquin**[4], **Rajesh V. Chopdekar**[5], **Nobumichi Tamura**[5], **James C. Weaver**[6], **Jun A. Y. Zhang**[1], **Stefano Goffredo**[7], **Giuseppe Falini**[8], **Matthew A. Marcus**[5], **Tamás Pusztai**[3], **Vanessa Schoeppler**[9], **Tali Mass**[4], **Pupa U. P. A. Gilbert**[1,10,§,*]

[1]Department of Physics, University of Wisconsin, Madison, WI 53706, USA

[2]Materials Science Program, University of Wisconsin, Madison, WI 53706, USA

[3]Institute for Solid State Physics and Optics, Wigner Research Centre for Physics, PO Box 49, 1525 Budapest, Hungary

[4]University of Haifa, Marine Biology Department, Mt. Carmel, Haifa 31905, Israel

[5]Advanced Light Source, Lawrence Berkeley National Laboratory, Berkeley, CA 94720, USA

[6]Wyss Institute for Biologically Inspired Engineering, Harvard University, Cambridge, MA 02138, USA

[7]Marine Science Group, Department of Biological, Geological and Environmental Sciences, University of Bologna, Via Selmi 3, I-40126 Bologna, Italy

[8]Department of Chemistry “Giacomo Ciamician”, Alma Mater Studiorum – University of Bologna, Via Selmi 2, 40126 Bologna, Italy

[9]B CUBE–Center for Molecular Bioengineering, Technische Universität Dresden, 01307 Dresden, Germany

[10]Departments of Chemistry, Geoscience, Materials Science, University of Wisconsin, Madison, WI 53706, USA

Abstract

Spherulites are radial distributions of acicular crystals, common in biogenic, geologic, and synthetic systems, yet exactly how spherulitic crystals nucleate and grow is still poorly understood. To investigate these processes in more detail, as a model system we chose corals, which are well known to form their skeletons from aragonite ($CaCO_3$) spherulites, and because a comparative study of crystal structures across coral species has not been performed previously. We observed that all 12 diverse coral species analyzed here exhibit plumose spherulites in their skeletons, with well-defined centers of calcification (CoCs), and crystalline fibers radiating from them. In 7 of the 12 species, we observed a skeletal structural motif not observed previously: randomly oriented, equant crystals, which we termed “sprinkles”. In *Acropora pharaonis*, these

*Correspondence to: pupa@physics.wisc.edu.
§previously publishing as Gelsomina De Stasio

Europe PMC Funders Author Manuscripts

sprinkles are localized at the CoCs, while in 6 other species sprinkles are either layered at the growth front (GF) of the spherulites, or randomly distributed. At the micro-scale, coral skeletons fill space as much as single crystals of aragonite. Based on these observations, we tentatively propose a spherulite formation mechanism in which growth front nucleation (GFN) of randomly oriented sprinkles, competition for space, and coarsening (either by Ostwald or Smoluchowski ripening) produce spherulites, rather than the previously assumed slightly misoriented nucleations termed “non-crystallographic branching”. Phase-field simulations support this mechanism, and, using a minimal set of thermodynamic parameters, are able to reproduce all of the microstructural variation observed experimentally in all of the investigated coral skeletons. Beyond coral skeletons, other spherulitic systems, from aspirin to semicrystalline polymers and chocolate, may also form according to the mechanism for spherulite formation proposed here.

Keywords

Crystal nucleation; crystal growth; coral; spherulite; sprinkle; polymer; semicrystalline; *Stylophora*; *Balanophyllia*; *Oculina*; *Phyllangia*; *Turbinaria*; *Acropora*; *Madracis*; *Porites*; *Favia*; *Blastomussa*; *Montipora*; *Micromussa*

1 Introduction

Spherulites comprise acicular crystals radiating from common centers. They are widespread and can be formed in metals [1], polymers or organic molecules [2–5], minerals crystallizing from melts [6, 7], and biominerals, including eggshells [8], otoliths [9], kidney stones [10], and coral skeletons [11, 12]. While it is well known that spherulites grow into spheres at micron, millimeter, or even centimeter scales [5, 13], the nucleation and growth mechanisms at the nanometer scale are poorly understood. Early studies from the late 1800s and early 1900s recognized that spherulitic structures analogous to those observed geologically were observed in coral skeletons [14, 15], but were suggested to be simply physicochemical results of “competition for space” during crystal growth [16]. Other studies investigating coral skeletal formation, revealed that organics, including proteins [17, 18] and polysaccharides [19, 20], play important roles in the nucleation, polymorph selection [21], crystal morphology, and orientation [22, 23]. Exactly how crystals form spherulites in coral skeletons thus remains unsettled.

In order to gain insight into the fundamental formation mechanism of spherulitic crystal growth, in the present study we analyzed the skeletons of a wide range of morphologically diverse, and distantly related scleractinian corals, also known as stony corals, because they form hard aragonite ($CaCO_3$) skeletons.

At the centimeter scale, the skeletons of scleractinian corals are morphologically diverse: they can be massive as in *Favia* sp. and *Porites* sp., branching as in *Stylophora* sp. and *Acropora* sp., encrusting as in *Phyllangia* sp. and *Oculina* sp., or table-like as in *Turbinaria* sp. At the microscopic scale, however, all modern stony coral skeletons reveal morphological similarities, displaying needle-like aragonite crystal fibers radiating from centers of calcification (CoCs) [16, 24–32], and forming plumose spherulites [11, 22, 33–36].

Europe PMC Funders Author Manuscripts

Historically, spherulites have been defined as a radial distribution of acicular crystals with a common center point, forming a spherical geometry. The center, however, does not have to be a single point; it can be a straight or curved line, or even a two-dimensional surface.

If the centers are along lines or surfaces, spherulites are termed “plumose”, as their cross-sections resemble plumes or feathers. Despite their name, in three-dimensions, plumose spherulites resemble bottle brushes or feather dusters, more than single, two-dimensional feathers. In coral skeletons, the spherulites observed here and previously are plumose spherulites.

A variety of methods have been used to characterize coral spherulites, all demonstrating that CoCs have a micro-granular structure [37–39], and in contrast to their adjacent aragonitic fibers, contain both aragonite and a stable amorphous calcium carbonate, and greater concentrations of magnesium and organics [19, 40–45].

Although all previous studies of coral skeletal fibers observed and described the radial distribution of their crystal long axes, there are, thus far, only two reports (from *Porites* sp. and *Stylophora pistillata* [11, 12]) describing, quantitatively, their precise crystal orientation directions and thus confirming unambiguously that coral skeleton growth in these two species is indeed spherulitic. Due to this limited sample size, however, several questions regarding the details of coral skeleton formation remain:

- **a.** Do other corals also form their skeletons spherulitically or are there alternative growth modes?
- **b.** Are the *c*-axes of aragonite crystal fibers oriented along the radial growth direction?
- **c.** How do spherulites grow? Can we learn new insights from the study of a diverse set of coral skeletons regarding how spherulitic growth occurs?
- **d.** If so, can the insights be generalized beyond coral skeletons to other materials systems?

The answers to the first two questions above are not as trivial as they might appear, based exclusively on the morphology of coral skeletons. To illustrate this point in a different biomineral system, in human enamel it was long established that nanocrystals in each enamel rod are elongated, parallel to one another, and co-oriented. Recent analysis, however, demonstrated that those morphologically parallel crystals are not at all co-oriented, nor is the *c*-axis of each nanocrystal oriented along the crystal’s long axis [46]. To a much smaller extent, this effect was also observed in parrotfish teeth [47]. In contrast, in synthetic hydroxyapatite spherulites, and synthetic [11] and biogenic aragonite spherulites [48], the *c*-axes are oriented along each crystal’s long axis [49]. Together, these results obtained from different crystal systems demonstrate that crystal long axes and *c*-axes are not necessarily parallel.

To avoid confusion, and from this point forward, crystallites of any kind will be called “grains” to conform with the common materials science terminology. In coral skeletons,

these grains are the micro- or nano-crystals usually termed fibers or CoCs by coral researchers.

Much of the confusion regarding the spherulitic growth of coral skeletons stems from the observation that the outer surface, which is the growth front of a coral skeleton, may or may not be spherulitic in morphology [20, 50, 51]. For example, Figure 1 shows scanning electron microscopy (SEM) images of corallites from three distantly related coral genera (Fig. S1). Despite the fact that the bulk, mature skeletons exhibit a distinctly spherulitic morphology, the growth fronts may vary from the smooth and disordered *Cyphastrea* sp. to the well-defined particle-like crystallites of *Balanophyllia* sp. (Fig. 1). Previous studies on the ultrastructure of sectioned coral skeletons using SEM and TEM [12, 48, 52], Polarized Light Microscopy (PLM) [22, 36], and Electron Back Scatter Diffraction (EBSD) [53, 54], however, have only revealed the presence of spherulitic aragonite, with no indication of the presence of these smaller-scale particulate features. Thus, the goals of the present study (questions a. and b.) are to investigate the potentially widespread nature of this particle-like skeletal structural motif, identify key skeletal maturation pathways (questions c. and d.), and attempt to reconcile the particles at the skeleton growth front described here (Fig. 1) with those reported previously [20, 51, 55, 56] and their proposed formation mechanism. To address these questions, we present here 60-nm resolution, large area (up to 200 × 300 μm^2), crystal orientation maps acquired with Polarization-dependent Imaging Contrast (PIC) mapping, which uses PhotoEmission Electron spectroMicroscopy (PEEM) [11, 57–61], from the skeletons of 12 distantly related and morphologically diverse coral species. The results obtained from these structural characterization studies will also be used to validate contrasting hypotheses related to growth front nucleation (GFN), an umbrella term that includes all possible microscopic mechanisms that lead to the formation of grains of new orientations at the growth front [62]. Historically, nucleation of crystals with slight misorientation has been called “non-crystallographic branching” (NCB), and has been assumed to explain how spherulitic crystals nucleate and grow [3, 4, 63, 64]. These mechanisms, however, still need experimental verification, and this paper is aimed at addressing precisely this point using coral skeletons as a model system.

2 Materials and Methods

Detailed materials and methods are provided in Appendix A. Briefly, coral skeletons (A.1) were embedded, polished, coated as described previously [65], and imaged on the PEEM-3 beamline 11.0.1.1 at the Advanced Light Source, LBNL, Berkeley, CA. Stacks of PEEM images were acquired at the oxygen K-edge π^* peak energy (534 eV), while rotating the linear polarization [11] to produce PIC maps using Igor Pro® (WaveMetrics, Lake Oswego, OR) and the Gilbert Group (GG) Macros [66] (A.2,3). Radiation damage to the samples was not observed in any of the PIC mapping experiments [58, 67–69]. Other methods like SEM, DNA, BET, μXRD, and EPMA analyses are also described in Appendix A.3-A.8 and phase-field simulations in A.9.

2.1 How to read a PIC map

Figures 2a and b show representative PIC maps of two coral skeletons across large areas, from two distantly related species: *Stylophora pistillata* (*Sp*) and *Balanophyllia europaea* (*Be*) acquired from the locations shown in the PLM images in Figures S2-S3. Colors in PIC maps, including hue and brightness, quantitatively display the azimuthal and polar angles of the *c*-axis with respect to the polarization plane, which is 60° from the image plane. The crystal *c*-axis projected onto the polarization plane is termed the c'-axis [11, 58], and its c' angle is quantitatively displayed by the hue in the color bar in Figure 2c: vertical in-plane (with respect to the polarization plane) is defined as 0° (cyan), clockwise and counterclockwise rotations from 0° are positive and negative angles, respectively, and horizontal in-plane is +90° or -90° (both red). The sample is mounted vertically, and the synchrotron x-ray beam illuminates the sample from the right at a grazing incidence angle of 30°. The polarization plane, perpendicular to the beam, is therefore rotated 60° with respect to the sample surface and intersects it along the vertical. Cyan crystals with their *c*-axes at 0°, therefore, have their *c*-axes in-plane in both the image and the polarization plane, but crystals with negative angles have *c*-axes coming out of the image plane at an angle of 60° from it and positive ones have their *c*-axes going in behind the image plane at an angle of 30°. The brightness corresponds to the off-plane angle, again with respect to the polarization plane, with 100%-brightness color indicating in-plane and 0% brightness (black) indicating 90° off-plane [58, 59]. Black crystals, therefore, have their *c*-axes directed into the beam.

2.2 Phase-field simulations

Phase-field simulations were performed using a phase-field model that incorporates growth front nucleation (GFN) [70, 71] specially designed to describe the formation of complex polycrystalline structures in polymers and alloys as described in Appendix A.9. The model, adopted here with modifications, describes the formation of new crystal grains, misaligned with respect to the parent crystal. The frequency and orientation of GFN events is governed by the relative magnitudes of the rotational and translational diffusion coefficients, D_{rot} and D_{trans}. D_{rot} determines how easy it is for a molecular unit to rotate around its axis and is associated with the geometry of the molecular unit, whereas D_{trans} determines how easy it is for the molecular unit to travel through the liquid medium towards the growth front. Therefore, the ratio of $D_{\mathrm{rot}}/D_{\mathrm{trans}}$ determines how misaligned the molecular unit is when it arrives at the growth front and solidifies. Accordingly, high $D_{\mathrm{rot}}/D_{\mathrm{trans}}$ ratio results in epitaxial growth, whereas low $D_{\mathrm{rot}}/D_{\mathrm{trans}}$ ratio results in randomly oriented grains as shown in Appendix A.9.3 and Figure A.9.

3 Results and Discussion

3.1 Expected aragonite spherulite structures in PIC maps

In *Sp* (see Table 1 for this and all other coral species abbreviations) bulk skeletons, aragonite crystal fibers form spherulitic bundles, as shown in Figure 2a. In each spherulite bundle, acicular crystal fibers always have their *c*-axis oriented along the long axis of the crystal, and adjacent crystal fibers are always only slightly misoriented with respect to their neighboring fibers, with angular distance of *c*-axes across grain boundaries smaller than 35°, which is a characteristic of spherulites, and in PIC maps corresponds to similar colors in adjacent fibers

(Fig. 2a). The CoCs appear nanoparticulate and exhibit similar adjacent colors. Abrupt color changes, therefore, are only observed at the boundaries of two spherulitic bundles (Fig. 2a). In Figure 2a the fibers labeled "F" are red, cyan, or magenta, indicating that their *c*-axes are nearly perpendicular to the image plane, parallel to it and vertical, or parallel and rotated in-plane, respectively. Even where the fibers do not appear elongated, e.g. the red fibers labeled F in Figure 2a, they are indeed elongated, but observed here in cross-section. All other 11 species had similar spherulitic structures to *Sp* in their skeletons (Figs. 3-6 and Figs. S2-S5). Thus, fibers in coral skeletons are spherulitic, and their *c*-axes are invariably oriented along the long axis of the fiber, as expected from extensive morphological studies [16, 26, 27, 29–31, 39, 72–74] as well as crystal orientation ones [11, 12, 53, 75].

3.2 Characterization of randomly oriented crystals termed "sprinkles"

In addition to spherulitic fibers and CoCs, *Be* shows crystals with abrupt change of colors across grain boundaries, interspersed with spherulitic crystal fibers, and ranging in size between 0.2 – 20 μm, (Fig. 2b). We termed these crystals "sprinkles", as they are reminiscent of colorful sugar sprinkles on cupcakes. Sprinkles are equant, that is, not elongated, untextured, and randomly oriented with respect to their neighboring grains. The angular distance of *c*-axes (Δc) across grain boundaries is narrowly distributed for spherulitic crystal fibers (Δc = 0°-35°), but randomly distributed for sprinkles (Δc = 0°-90°), as shown in Figures 2d,e. Multiple areas per sample, and several samples of *Sp* and *Be* from different skeletons were analyzed, all confirming that the results in Figure 2 are representative and reproducible.

3.2.1 Sprinkles are observed in coral skeletons of 7 out of 12 coral species—

To determine whether sprinkles are unique to *Be* or common to other species, we examined additional coral skeletons from different coral clades (robust or complex)[76], different growth morphologies (branching, solitary, encrusting, table-like, or massive), and of different geographic origins (Indo-Pacific, Red Sea, and Mediterranean Sea). The 12 species analyzed are listed in Table 1, along with the abbreviation of their genus and species, their clade, morphology, geographical origins, and climates. The phylogenetic tree for all 12 species is presented in Figure S1.

Out of the 12 species analyzed, 7 species exhibited sprinkles. Of these, 3 exhibited only small sprinkles (0.2-2.0 μm, *Pam, Op, Ap*) (Fig. 3), 2 showed only large sprinkles (2-20 μm, observed in *Mp, Fs*) (Fig. 4), and 2 showed both small and large sprinkles (*Be*, *Bm*)(Figs. 2b, 3, and 4). Small and large sprinkles, e.g. the ones indicated by arrows in Figs. 3 and 4, have very different colors at their boundaries, e.g. complementary colors such as red and cyan, or green and magenta, or blue and yellow, thus they are misoriented sprinkles. Five out of 12 species showed no sprinkles, or so few that they could not be unambiguously interpreted as sprinkles: they could have been fibers from other spherulites either in front or behind the analyzed polished surface. The species with no sprinkles include *Sp, Tp, Pl, Mt*, and *Ml* (Fig. 5).

3.2.2 Sprinkles are equant and are not fibers from other spherulites—

We stress that sprinkles in *Be, Bm, Pam*, *Op*, *Ap, Mp and Fs* are never elongated, therefore they

must be approximately equant, unlike the fibers that are always elongated. If sprinkles were elongated, observing thousands of them as presented here (Figs. 2b, 3, 4 and others) should show at least a few with their long axis randomly oriented but lying in plane and thus appearing elongated. Since such randomly oriented, elongated crystals never appeared in any of the PIC maps, we conclude that sprinkles are equant.

Furthermore, since the sprinkles observed in *Be, Bm, Pam*, *Op*, and *Ap* are randomly oriented, they cannot be fibers from other spherulites in front or behind the image plane. If they were, they would have colors different from the main spherulite imaged, but similar to one another. The observed random distribution of colors (e.g. Fig. 2e) implies that, if sprinkles were fibers from other spherulites, they would have to belong to tens of different spherulites, which is geometrically impossible.

In a few PIC maps, a small set of differently oriented crystals do appear at the boundaries between two spherulite bundles of fiber crystals (e.g. arrows in *Pl, Mt, Ml* Figs. 5d,e,f). These sprinkles are so few that they could be from 1 or 2 other spherulites in front or behind the image plane. We therefore conservatively placed *Pl, Mt, Ml* in the sprinkle-free group.

3.2.3 Sprinkles are made of aragonite, with higher Na and Mg—Powder X-ray diffraction (XRD) analysis of bulk *Be* skeletons (Fig. S6) and X-ray absorption near edge structure (XANES) spectroscopy at the Ca L-edge acquired selectively from sprinkles and fibers in *Be* skeletons (Fig. S7) and fibers in *Sp* skeletons identified aragonite as the sole crystalline polymorph in sprinkles and fibers alike [58].

Electron Probe MicroAnalysis (EPMA), however, showed that sprinkles contain significantly more Na and Mg, and less Sr than spherulitic crystal fibers (Table S1). The higher amount of Mg and therefore Mg/Ca ratio has been observed before in the CoCs of various coral species [77–79], and may be associated with organics, an amorphous phase [80], or increased local pH [81]. Under the experimental conditions employed here, sprinkles are identified as fully crystalline aragonite, and thus the local variation in Mg incorporation may be related to the presence of different concentrations of intracrystalline Mg-binding macromolecules [21].

Synchrotron X-ray micro-diffraction (μXRD), done in monochromatic powder diffraction mode, showed that in the aragonite {111} family of planes, the *d*-spacing is 0.05 ± 0.02% larger in sprinkles than in spherulitic fiber crystals (Fig. S8), which is also consistent with the presence of organics in sprinkle aragonite [82]. Because all *Ap* skeletons have sprinkles only at CoCs (Fig. 3d, 6) and the vertical black line in Figure S8 is definitely a line of CoCs, we can confidently interpret the μXRD data transect as spanning spherulitic fibers on the left, CoC-sprinkles, and again fibers on the right.

3.2.4 Sprinkles are not easily recognizable in SEM images—In all previous studies of coral skeletons from all species, the skeletons were observed to grow as spherulites, thus the observation of a different non-spherulitic structure, the sprinkles, was unexpected. Interestingly, SEM images of etched mature *Be* skeletons, such as those in Figure S9, show spherulitic crystals, and where crystals are not acicular and radially

distributed, the parsimonious interpretation is that they are still spherulitic and acicular but oriented perpendicular to the imaging plane. It is also possible that, because the small sprinkles are 0.2-2.0 μm, they could be mistaken for fragmented fibers in fractured samples, or they could be dissolved preferentially in partially etched samples. It is therefore not surprising that previous reports, based solely on morphological studies of sectioned, fractured, or etched coral skeletons, did not describe sprinkles. The results presented here, in contrast, demonstrate that crystal orientation analysis is useful to identify sprinkles and distinguish them from off-plane sectioned spherulites.

3.2.5 Can sprinkles be fusiform crystals?—Previous SEM studies of coral skeleton growth described "fusiform crystals" in a variety of species, including *Acropora cervicornis* [83], *Pocillopora damicornis* [84, 85], *Galaxea fascicularis* [86, 87], and *Sp* [88]. These were 0.3-3 μm spindle-shaped crystals, observed at the surface of the growing skeleton, and interpreted as early-stage depositions in coral skeleton formation, distinct from acicular aragonite crystal fibers [83]. Although their size is similar to the small sprinkles found in PIC maps, fusiform crystals were never reported to appear in the bulk of mature coral skeletons, thus they may or may not be sprinkles. Sprinkles never appear fusiform in shape, so it is difficult to conclude with certainty that fusiform crystals become sprinkles, once they are incorporated into the growing skeleton. But their equant, random shape may be due to their observation here within the skeleton, and therefore at a later developmental stage.

3.2.6 Sprinkles are not CoCs, in general, but are CoCs in *Acropora* —The small sprinkles observed in *Be, Pam, Op* cannot be CoCs, because acicular crystal fibers radiating from them were never observed. Furthermore, in most species, wherever CoCs were recognizable by their characteristic nanoparticulate structure and by the fibers radiating from them, CoC nanocrystals were not randomly oriented, but rather, neighboring crystals had similar orientations (Figs. 2a, 3e, 4c,e, 5b,c,d,e).

In one species only, *Ap*, randomly oriented sprinkles were co-localized with CoCs (Fig. 3d, 6), they were arranged along lines, and fibers radiated from sprinkles instead of CoCs. One could, therefore, conclude that sprinkles are the first nucleated crystals, and occur only at the CoCs, but this interpretation does not hold for the other 11 species analyzed here.

3.2.7 Sprinkles are at the growth front (GF) of spherulitic bundles in *Be* and *Op* —In all species, sprinkles are interspersed with spherulitic crystal fibers. They are observed in distantly related species, therefore, they are a broadly occurring crystal growth mode in coral skeletons. In two regions of *Be* and *Op* skeletons, sprinkles appear to be layered around the GF of fanning spherulitic fiber crystals (Figs. 3c,e, between pairs of GF labels). This observation is consistent with GFN of sprinkles, which then either become fibers or are trapped as sprinkles, as described below.

3.3 Concentric rings in *Acropora*

In addition to sprinkles, spherulitic fibers, and CoCs, the *Ap* skeleton showed a fourth micro-scale structure – concentric rings approximately 5 – 20 μm apart, labeled "R" in Fig. 6a and magnified in Fig. 6b. Among the 12 species analyzed here, these concentric rings

were only observed in *Ap*, and while these features were previously described in other *Acropora* species, they have not yet been fully characterized [36, 89, 90].

The concentric rings are composed of elongated slightly misoriented nanocrystals, as confirmed by the distribution of Δc in Figure 2d, and thus, according to the quantitative definition introduced by Sun *et al.* [11] they are spherulitic. However, unlike previously known spherical or plumose spherulites that form fanning bundles of fibers (Fig. 2a, and middle of Fig. 6a), they instead form curved layered structures. From the literature, these concentric rings are likely cross-sections of small protrusions on the skeleton surface, termed “spiniform trabeculae” [89] or “shingles” [36]. Interestingly, unlike spherulitic crystals fanning from CoCs, the nanocrystal domains in the concentric rings do not seem to coarsen as they grow, further confirming that the concentric rings are a distinct structure compared to plumose spherulite fibers radiating out of CoCs.

3.4 Coral skeleton are completely space-filling

To measure whether or not coral skeletons are space-filling, and if so, how much, we used the Brunauer-Emmett-Teller (BET) method [91, 92]. As shown in Table 2, the specific surface area of powdered coral skeletons from *Sp* and *Be* indicates that they are as space-filling as single crystals of geologic aragonite.

3.5 Hypothesis: sprinkles are proto-fibers

Since sprinkles formed in distantly related species are identical in mineral phase to spherulitic crystal fibers, and are interspersed with fibers, we tested the hypothesis that sprinkles are proto-fibers, that is, that they are the first-nucleated seed of each crystalline fiber in a spherulite, and that the existence of sprinkles involves thermodynamic and kinetic controls of the crystallization process during coral biomineralization.

In coral skeletons as well as other spherulitic crystal systems, the nanoscale mechanism by which a new, differently oriented crystal is nucleated and then either grows or shrinks remains unknown (questions c. and d), despite recent efforts [93]. New nucleation events, however, must occur all the time during spherulitic growth, not only at the center of a sphere or at the CoCs, but everywhere, in order to fill space. Otherwise, acicular crystals would diverge from one another as spokes on a wheel, with increasingly large gaps between crystals. This is never the case in spherulites, whether biogenic (see Table 2 and [92]), geologic, or synthetic: spherulites are always space-filling.

We propose that randomly oriented crystals, such as the sprinkles observed here, solve this problem: they are the first-nucleated, initially randomly oriented seeds of fiber crystals, which, if they are nearly co-oriented with their neighboring crystals, have space to grow larger radially, if not, they do not, run into one another during growth and remain smaller. In the first case, the sprinkle is a proto-fiber, in the second it is mis-oriented. We tentatively propose that a coarsening process makes small, mis-oriented sprinkles disappear. Occasionally, in 7 of the 12 coral species, either the organics likely trapped in sprinkles, or other mechanisms, stabilize the sprinkles and make them resist the coarsening process, which, we further hypothesize, occurs spontaneously, and is therefore common to biogenic, geologic, and synthetic spherulitic growth. The randomly oriented sprinkle seeds observed

here do not nucleate in any mechanism previously observed or simulated. In the data presented, sprinkles are frequently nucleated at all distances from spherulite centers, the CoCs, thus a mechanism that includes and explains their existence is necessary.

3.6 Growth front nucleation (GFN) in coral skeletons

The sprinkles observed in *Be* and *Op* are preferentially localized along growth fronts as presented in Figs. 3c,e. This suggests that GFN occurs in coral skeletons, and that sprinkles are the first nucleated crystals at the GF. The main technique used to model GFN in this paper is phase-field simulation using a phase-field model incorporating GFN [70, 71], briefly described in section 2.2 and in greater detail in Appendix A.9.

3.7 Proposed spherulitic growth mechanism: GFN of sprinkles

Based on the observation of sprinkles at GFs, and the hypothesis that sprinkles are proto-fibers, here we propose a mechanism for the growth of spherulites that includes and explains sprinkles. The mechanism of spherulite growth we propose is summarized in Figure 7, and it has four stages:

1. Randomly oriented sprinkles nucleate from a liquid or an amorphous solid, immediately outside the liquid-solid interface or inside of it at the expense of an amorphous precursor solid [94]. In corals, the interface is the surface of the growing coral skeleton, and nucleation of sprinkles occurs within the amorphous solid, near the surface, but inside of it by a few microns. Fig. S10 substantiates this expectation.
2. Aragonite crystals, or any other spherulite-forming crystals, grow preferentially along the *c-ax*is, thus the aspect ratio of sprinkle nuclei increases, and the crystals become acicular. In corals skeletons, they become fibers, which grow at the expense of the amorphous precursors.
3. During this growth, sprinkles with their c-axes radially oriented have space to elongate, whereas transverse ones run into one another and thus remain small. The result is spherulitic growth of acicular crystal fibers with slight misorientation across grain boundaries. This growth mechanism concurs with Barnes's competition for space model [16], and with Gladfelter's hypothesis that randomly oriented fusiform crystals are the first to be deposited [83]. The latter concurs with sprinkles, if fusiform crystals and sprinkles are the same entities. The nucleation and space filling of sprinkles and fibers concur with the classical understanding of polycrystalline 3D-solid or 2D-film formation [95].
4. Finally, sprinkles with their c-axes radially oriented grow into larger fibers and other non-radially oriented sprinkles shrink. In this coarsening process, radial sprinkles grow at the expense of non-radial, smaller ones. In corals, the coarsening process occurs in the bulk of the skeleton, once all or most of the skeleton has solidified and filled space. If the skeleton surface is not yet space-filling, but still porous at the time of coarsening, the calcifying fluid between the cells and the growing skeleton [96] may facilitate the dissolution and re-precipitation of smaller sprinkles and coarsening of the larger, radially oriented

Europe PMC Funders Author Manuscripts

Europe PMC Funders Author Manuscripts

ones [97, 98]. If it is already space-filling, then coarsening could be an entirely solid-state transformation, akin to the coarsening of polycrystalline metals such as Ag and Pt that can occur at room temperature [99, 100]. Coarsening in liquid or solid phases is well-established in classical crystallization, and usually termed Ostwald ripening [97, 98] or Smoluchowski ripening [99, 100], respectively.

During coarsening, small sprinkles shrink and disappear, whereas spherulitic crystals grow larger. This mechanism explains why random orientations are usually not observed in spherulites: by the time a spherulite is fully formed and coarsened, it no longer contains sprinkles. Occasionally, however, sprinkles are retained.

Such a thermodynamically driven skeletal growth process has been described in *Pinna nobilis* prismatic calcite [101], whose grains coalesce according to classical metallurgical theory [102], or in the aragonitic shells of *Unio pictorum, Nautilus pompilius*, and *Haliotis asinina*, whose ultrastructure gradually transitions from a randomly aggregated, to a prismatic, to a nacre layer, through a directional solidification process [103, 104], as occurs in metals.

3.8 Compatibility with amorphous precursors

It is known that coral skeletons grow at the expense of amorphous precursors [94]. The space-filling of sprinkles and fibers discussed here, and their coarsening, are invariant whether the crystals grow at the expense of ions from solution, a dense liquid precursor, or a space-filling solid amorphous precursor. The concepts proposed here are purely geometric, and thus not affected by these three distinct scenarios for coral skeleton formation. Nucleation and growth throughout this paper refer to a new crystal orientation, not to an amorphous solid nucleating and growing from liquid solution.

3.9 Phase-field simulations support the proposed formation from proto-fiber sprinkles

To test the hypothesis that sprinkles are the first nucleated crystals at the GF, and that they grow and coarsen if they are radially oriented but are sometimes retained as observed in coral skeletons, we performed a phase-field simulation in which sprinkles are deposited first, and then grow competitively. We used the spherulite model in Gránásy et al. [105], but omitted the local minimum in grain boundary energy that would force GFN with a given misorientation, and would thus yield a fixed mis-orientation angle. In our simulation, therefore, GFN of sprinkles occurs with random orientation. The simulations were performed in two dimensions, and we applied a large two-fold symmetry for the solid-liquid interface energy, which yields elongated growth shapes mimicking aragonite crystals. Remarkably, not only did the crystals in the simulations grow into a spherulite with small grain boundary angles, but there were also sprinkles scattered within the spherulite, as shown in Figure 8. With time, some of the sprinkles formed during GFN remained sprinkles (Fig. 8, white boxes), whereas others disappeared due to competitive grain coarsening (Fig. 8, black boxes). Both observations are consistent with the PIC mapping data presented here for coral skeleton spherulitic fibers and sprinkles. The coarsening, proposed and tested here, could involve dissolution and recrystallization of the sprinkles at the solid-liquid interface, but could also happen within the solid, where shrinking grains minimize surface energy (Ostwald or Smoluchowski ripening). Grain boundaries are disordered, in the phase-field

simulation they are regions with higher, liquid-like mobility, and thus facilitate re-orientation of the units at the periphery of a sprinkle as the sprinkle shrinks and eventually disappears. In the case of coral skeletons, the re-orientation of sprinkles can occur as dissolution and reprecipitation from the calcifying fluid, and Ostwald ripening, or as grain shrinking, enabled by the sparing amount of water released by dehydration of hydrated amorphous calcium carbonate nanoparticles. Such hydrated nanoparticles are present in the forming skeleton and surrounded by crystalline aragonite, as shown by Mass et al. [94]

In a previous study, Sun et al. analyzed aragonite spherulites synthesized at room temperature and 1 atm in the absence of any organic molecules, and never found any sprinkles [11]. Thus, the D_{rot} of aragonitic $CaCO_3$ molecular units typically falls in a range that allows certain frequencies and misalignments of GFN to favor spherulitic structures to form at ambient conditions. For sprinkles to persist, instead, D_{rot} must be smaller, so sprinkles can form via GFN without matching their orientations to the mother crystal. Such small D_{rot} could be induced by binding of organic molecules to $CaCO_3$ molecules or particles, and/or the presence of trace element impurities. This possibility is supported by the fact that electrophoretic analyses of coral skeletal organic matrices [19, 106] exhibit variability between species. The size and shape of spherulitic aragonite crystals also varies across different taxa and species [22, 107]. Thus, in different coral species D_{rot} is likely different.

3.10 Simulations support all of the experimentally observed structures

In summary, the theoretical phase-field simulation in Figure 8 shows strong similarity with the proposed mechanism: small sprinkles originate through GFN, then recrystallize in a coarsening process and thus, we argue, are not observed in many coral skeletons (Fig. 5, *Sp, Tp, Pl, Mt, Ml*) presumably because these have a larger $D_{\mathrm{rot}}/D_{\mathrm{trans}}$ ratio. Coral skeletons that retain small sprinkles (Fig. 3, *Bm, Pam, Op, Ap, Be*), instead, presumably have a smaller $D_{\mathrm{rot}}/D_{\mathrm{trans}}$ ratio. A variety of such $D_{\mathrm{rot}}/D_{\mathrm{trans}}$ ratios is presented in Appendix A, Figure A.9.

The simulation of Figure 9a shows that a branched structure can grow, in which the center of each branch resembles *Ap* coral skeletons (Figs. 2d, 6, 9, S5, S8, S11) with sprinkles along CoCs, whereas the larger crystals on the outside of each branch are similar to the large sprinkles (2-20 μm) observed in some skeletons (Fig. 4, *Bm, Mp, Fs, Be).* The simulations presented here, therefore, are able to reproduce all the observed structural features found in real coral skeletons.

3.11 Additional support for GFN of sprinkles in fresh, forming *Stylophora pistillata*

In addition to theoretical simulations, an independent line of evidence suggests initial GFN of sprinkles: Figure S10 shows that, near the surface of *Sp* skeletons, randomly oriented sprinkles can be retained. These were only observed in fresh forming skeletons near the growth front, whereas in the mature *Sp* skeletons, only spherulitic crystal fibers and CoCs were found (Figs. 2a, 5c). The presence of sprinkles near the GF in a fresh, forming *Sp* coral skeleton (Fig. S10) and their absence in the mature *Sp* skeletons (Figs. 2a,5c) is the only experimental evidence that sprinkles disappear, and is only indirect evidence.

3.12 Possible relevance to other biomineral systems

Other biominerals have been previously observed to have nearly co-oriented neighboring crystals, including mollusk shell nacre [108] and calcite prisms [109], and ascidian (tunicate) spicules [59]. The growth mechanism described here, including competition for space and coarsening, may be relevant to other geometries, completely different from spherulitic crystals. But this must be demonstrated in future work, beyond the scope of the present paper. The same growth mechanism may also apply to biomimetic spherulites [110].

3.13 Possible relevance to semicrystalline polymers

A variety of organic macromolecules or polymers used to make plastics, rubber, textiles etc., are partly crystalline and partly amorphous, and are therefore termed semicrystalline. The crystalline component is frequently spherulitic [111]. The degree of crystallinity, that is, what proportion of the polymers, after solidification, are crystalline and not amorphous is inversely proportional to the molecular weight of the polymers [112–114], as longer polymer chains are harder to fully crystallize. Raman spectroscopy is highly sensitive to the degree of crystallinity in bulk polymer materials [115–117], but it is most commonly employed for bulk analysis. Using spatially resolved Raman spectroscopy, Yang et al. recently studied the degree of crystallinity within single spherulites. They found that crystallinity is not evenly distributed, but lower near the center of each spherulite and increases with position along the spherulite radius [118]. The pattern of crystallinity thus has important implications for the melting point and the glass transition temperature of the polymer materials.

The mechanism tentatively proposed here may therefore also be relevant to semicrystalline polymer materials. In this case, the first-nucleated crystals would be randomly oriented polymer sprinkles, followed by crystal growth in competition for space, and coarsening. Arresting coarsening, perhaps through rapid freezing, may reveal sprinkles, detectable by Raman spectroscopy and visible by PLM.

In mesocrystalline polymer films, sprinkles are occasionally observed, interspersed with acicular spherulitic crystals (see figure 2B in ref. [95]). The acicular crystals grow and surround sprinkles, exactly as they do in coral skeletons (e.g. Fig. 2b arrows).

4 Conclusions

In summary, we analyzed the skeletons of 12 distantly related coral species and a key feature emerged: 7 of the 12 species exhibit 0.2-20 μm randomly oriented sprinkles. Even sprinkle-free corals, however, showed sprinkles near the skeletal growth front, and in all species examined, no correlation was found between the formation of sprinkles and either environmental factors or evolutionary history. The observation of sprinkles suggested a growth mechanism for spherulites, in which sprinkles are formed by randomly oriented GFN events, competition for space, and coarsening, and not through slightly misoriented nucleations as previously assumed for NCB. This mechanism is strongly supported by phase-field simulations, which explain the microstructural variations across species in terms of thermodynamic parameters, and their possible origin from differences in matrix organic molecules or trace element composition. In addition to providing new insights into the coral

biomineralization processes, this study may prove useful for spherulitic crystal growth in general, which occurs in many other systems including aspirin [119, 120], polymers [118], shrimp eyes [121], opal [122], graphite in cast iron [123], and cocoa butter in chocolate [124]. Thus, the spherulite formation mechanism proposed here may be applied to mineral and organic spherulites, natural and synthetic crystals, in the metallurgical, pharmaceutical, and food industries. Furthermore, this study provides evidence that interdisciplinary research combining experimental and theoretical techniques can be a particularly powerful approach for elucidating the fundamental mechanisms of crystal nucleation and growth.

Supplementary Material

Refer to Web version on PubMed Central for supplementary material.

Acknowledgements

We thank Andreas Scholl for his technical help during beamtime, Franklin Hobbs during powder XRD, John Fournelle for EPMA analysis, Carl I. Steefel and Wenming Dong for BET analysis. This work was 80% supported by the U.S. Department of Energy, Office of Science, Office of Basic Energy Sciences, Chemical Sciences, Geosciences, and Biosciences Division [Award DE-FG02-07ER15899 to PG], and 20% by NSF [grant DMR-1603192 to PG]. In addition, TM acknowledges support from the United States-Israel Binational Science Foundation [BSF Grant # 2014035], and from the European Research Commission [ERC Grant # 755876]. GF and SG thank the European Research Council under the European Union's Seventh Framework Programme [FP/2007-2013, ERC; Grant # 249930 – CoralWarm]. LG and TP acknowledge the support by the National Agency for Research, Development, and Innovation, Hungary [NKFIH Contracts No. KKP-126749 and K-115959]. All PIC maps were acquired at the Advanced Light Source, which is supported by the Director, Office of Science, Office of Basic Energy Sciences, US Department of Energy [Contract No. DE-AC02-05CH11231].

References

[1]. Geveling NN, Maslenkov SB. Solidification of eutectic Ni-Ni3Ti alloys. Metal Sci Heat Treatm. 1976; 18(9):755–760.

[2]. Padden FJ, Keith HD. Spherulitic crystallization in polypropylene. J Appl Phys. 1959; 30(10):1479–1484.

[3]. Shtukenberg A, Freundenthal J, Gunn E, Yu L, Kahr B. Glass-crystal growth mode for testosterone propionate. Cryst Growth Des. 2011; 11(10):4458–4462.

[4]. Shtukenberg AG, Hu CT, Zhu Q, Schmidt MU, Xu W, Tan M, Kahr B. The third ambient aspirin polymorph. Cryst Growth Des. 2017; 17(6):3562–3566.

[5]. Way J, Atkinson J, Nutting J. The effect of spherulite size on the fracture morphology of polypropylene. J Mater Sci. 1974; 9(2):293–299.

[6]. Fowler AD, Berger B, Shore M, Jones MI, Ropchan J. Supercooled rocks: development and significance of varioles, spherulites, dendrites and spinifex in Archaean volcanic rocks, Abitibi Greenstone belt, Canada. Precambrian Res. 2002; 115(1–4):311–328.

[7]. Peloquin AS, Verpaelst P, Ludden JN. Spherulitic rhyolites of the Archean Blake River Group, Canada; implications for stratigraphic correlation and volcanogenic massive sulfide exploration. Econ Geol. 1996; 91(2):343–354.

[8]. Hincke MT, Nys Y, Gautron J. The eggshell: structure, composition and mineralization. Front Biosci. 2012; 17(1266):120.

[9]. Parmentier E, Cloots R, Warin R, Henrist C. Otolith crystals (in Carapidae): Growth and habit. J Struct Biol. 2007; 159(3):462–473. [PubMed: 17616468]

[10]. Al-Atar U, Bokov AA, Marshall D, Teichman JMH, Gates BD, Ye Z-G, Branda NR. Mechanism of calcium oxalate monohydrate kidney stones formation: layered spherulitic growth. Chem Mater. 2010; 22(4):1318–1329.

[11]. Sun CY, Marcus MA, Frazier MJ, Giuffre AJ, Mass T, Gilbert P. Spherulitic growth of coral skeletons and synthetic aragonite: Nature's three-dimensional printing. ACS Nano. 2017; 11(7):6612–6622. [PubMed: 28564539]

[12]. Benzerara K, Menguy N, Obst M, Stolarski J, Mazur M, Tylisczak T, Brown GE Jr, Meibom A. Study of the crystallographic architecture of corals at the nanoscale by scanning transmission X-ray microscopy and transmission electron microscopy. Ultramicroscopy. 2011; 111(8):1268–75. [PubMed: 21864767]

[13]. Magill JH. Review spherulites: a personal perspective. J Mat Sci. 2001; 36(13):3143–3164.

[14]. Bryan WH, Hill D. Spherulitic crystallization as a mechanism of skeletal growth in the hexacorals. Procs R Soc Queensland. 1941; LII(9):78–91.

[15]. Ogilvie MM. Microscopic and systematic study of madreporarian types of corals. Phil Trans R Soc London Series B. 1896; 187:83–345.

[16]. Barnes DJ. Coral Skeletons: An Explanation of Their Growth and Structure. Science. 1970; 170(3964):1305–1308. [PubMed: 17829430]

[17]. Akiva A, Neder M, Kahil K, Gavriel R, Pinkas I, Goobes G, Mass T. Minerals in the pre-settled coral Stylophora pistillata crystallize via protein and ion changes. Nat Comms. 2018; 9(1)

[18]. Mass T, Drake JL, Peters EC, Jiang W, Falkowski PG. Immunolocalization of skeletal matrix proteins in tissue and mineral of the coral *Stylophora pistillata* . Procs Natl Acad Sci. 2014; 111(35):12728–12733.

[19]. Cuif J-P, Dauphin Y, Doucet J, Salome M, Susini J. XANES mapping of organic sulfate in three scleractinian coral skeletons. Geochim Cosmochim Acta. 2003; 67(1):75–83.

[20]. Falini G, Reggi M, Fermani S, Sparla F, Goffredo S, Dubinsky Z, Levi O, Dauphin Y, Cuif J-P. Control of aragonite deposition in colonial corals by intra-skeletal macromolecules. J Struct Biol. 2013; 183(2):226–238. [PubMed: 23669627]

[21]. Laipnik R, Bissi V, Sun C-Y, Falini G, Gilbert PU, Mass T. Coral acid rich protein selects vaterite polymorph in vitro. Journal of Structural Biology. 2019

[22]. Cuif JP, Dauphin Y. The two-step mode of growth in the scleractinian coral skeletons from the micrometre to the overall scale. J Struct Biol. 2005; 150(3):319–31. [PubMed: 15890280]

[23]. Reggi M, Fermani S, Landi V, Sparla F, Caroselli E, Gizzi F, Dubinsky Z, Levy O, Cuif J-P, Dauphin Y, Goffredo S, et al. Biomineralization in Mediterranean Corals: The Role of the Intraskeletal Organic Matrix. Cryst Growth Des. 2014; 14(9):4310–4320.

[24]. Wang H. A revision of the *Zoantharia Rugosa* in the light of their minute skeletal structures. Phil Trans R Soc London Series B. 1950; 234(611):175–246.

[25]. Wainwright SA. Studies of the mineral phase of coral skeleton. Exper Cell Res. 1964; 34(2):213–230.

[26]. Cuif J-P, Dauphin Y. Microstructural and physico-chemical characterization of ‘centers of calcification’in septa of some Recent scleractinian corals. Paläontologische Zeitschrift. 1998; 72(3–4):257–269.

[27]. Rollion-Bard C, Blamart D, Cuif J-P, Juillet-Leclerc A. Microanalysis of C and O isotopes of azooxanthellate and zooxanthellate corals by ion microprobe. Coral Reefs. 2003; 22(4):405–415.

[28]. Stolarski J. Three-dimensional micro-and nanostructural characteristics of the scleractinian coral skeleton: a biocalcification proxy. Acta Palaeontol Polon. 2003; 48(4)

[29]. Nothdurft LD, Webb GE. Microstructure of common reef-building coral genera Acropora, Pocillopora, Goniastrea and Porites: constraints on spatial resolution in geochemical sampling. Facies. 2007; 53(1):1–26.

[30]. Brahmi C, Meibom A, Smith D, Stolarski J, Auzoux-Bordenave S, Nouet J, Doumenc D, Djediat C, Domart-Coulon I. Skeletal growth, ultrastructure and composition of the azooxanthellate scleractinian coral Balanophyllia regia. Coral Reefs. 2010; 29(1):175–189.

[31]. Cuif, J-P, Dauphin, Y, Sorauf, JE. Biominerals and fossils through time. Cambridge University Press; 2010.

[32]. Shapiro OH, Kramarsky-Winter E, Gavish AR, Stocker R, Vardi A. A coral-on-a-chip microfluidic platform enabling live-imaging microscopy of reef-building corals. Nat Comms. 2016; 7

[33]. Cohen AL, Holcomb M. Why corals care about ocean acidification: uncovering the mechanism. Oceanography. 2009; 22(4):118–127.

[34]. Cohen AL, McConnaughey TA. Geochemical perspectives on coral mineralization. Revs Mineral Geochem. 2003; 54(1):151–187.

[35]. Holcomb M, Cohen AL, Gabitov RI, Hutter JL. Compositional and morphological features of aragonite precipitated experimentally from seawater and biogenically by corals. Geochim Cosmochim Acta. 2009; 73(14):4166–4179.

[36]. Nothdurft LD, Webb GE. Microstructure of common reef-building coral genera Acropora, Pocillopora, Goniastrea and Porites: constraints on spatial resolution in geochemical sampling. Facies. 2006; 53(1):1–26.

[37]. Constantz, B, Meike, A. Calcite centers of calcification in *Mussa angulosa* (Scleractinia), Origin, evolution, and modern aspects of biomineralization in plants and animals. Springer; 1989. 201–207.

[38]. Shirai K, Kusakabe M, Nakai S, Ishii T, Watanabe T, Hiyagon H, Sano Y. Deep-sea coral geochemistry: Implication for the vital effect. Chemical Geology. 2005; 224(4):212–222.

[39]. Wang H. A revision of the Zoantharia Rugosa in the light of their minute skeletal structures. Philosophical Transactions of the Royal Society of London Series B, Biological Sciences. 1950; 234(611):175–246. [PubMed: 24537107]

[40]. Ramseyer K, Miano TM, D'orazio V, Wildberger A, Wagner T, Geister J. Nature and origin of organic matter in carbonates from speleothems, marine cements and coral skeletons. Organic Geochem. 1997; 26(5–6):361–378.

[41]. Rollion-Bard C, Blamart D. DiMasi E, Gower LB. SIMS method and examples of applications in coral biomineralization. Biomineralization Sourcebook: Characterization of Biominerals and Biomimetic Materials. 2014:249–261.

[42]. Gautret P, Cuif J-P, Stolarski J. Organic components of the skeleton of scleractinian corals-evidence from in situ acridine orange staining. Acta Palaeontol Polon. 2000; 45(2):107–118.

[43]. Goffredo S, Vergni P, Reggi M, Caroselli E, Sparla F, Levy O, Dubinsky Z, Falini G. The skeletal organic matrix from Mediterranean coral *Balanophyllia europaea* influences calcium carbonate precipitation. PLoS One. 2011; 6(7):e22338. [PubMed: 21799830]

[44]. Ramseyer K, Miano TM, D'orazio V, Wildberger A, Wagner T, Geister J. Nature and origin of organic matter in carbonates from speleothems, marine cements and coral skeletons. Organic Geochemistry. 1997; 26(5–6):361–378.

[45]. Von Euw S, Zhang Q, Manichev V, Murali N, Gross J, Feldman LC, Gustafsson T, Flach C, Mendelsohn R, Falkowski PG. Biological control of aragonite formation in stony corals. Science. 2017; 356(6341):933–938. [PubMed: 28572387]

[46]. Beniash E, Stifler CA, Sun C-Y, Jung GS, Qin Z, Buehler MJ, Gilbert PUPA. The hidden structure of human enamel. Nat Comms. 2019; 10

[47]. Marcus MA, Amini S, Stifler CA, Sun C-Y, Frazier MJ, Tamura N, Bechtel HA, Parkinson DY, Barnard HS, Zhang XXX, Chua JQI, et al. Parrotfish teeth: stiff biominerals whose microstructure makes them tough and abrasion-resistant to bite stony corals. ACS Nano. 2017; 11(22):11856–11865. [PubMed: 29053258]

[48]. van de Locht R, Verch A, Saunders M, Dissard D, Rixen T, Moya A, Kroger R. Microstructural evolution and nanoscale crystallography in scleractinian coral spherulites. J Struct Biol. 2013; 183(1):57–65. [PubMed: 23685125]

[49]. Nassif N, Martineau F, Syzgantseva O, Gobeaux F, Willinger M, Coradin T, Cassaignon S, Azaïs T, Giraud-Guille M-M. In vivo inspired conditions to synthesize biomimetic hydroxyapatite. Chemistry of Materials. 2010; 22(12):3653–3663.

[50]. Cuif JP, Dauphin Y. The environment recording unit in coral skeletons – a synthesis of structural and chemical evidences for a biochemically driven, stepping-growth process in fibres. Biogeosciences. 2005; 2(1):61–73.

[51]. Coronado I, Pérez-Huerta A, Rodríguez S. Computer-integrated polarisation (CIP) in the analysis of fossils: a case of study in a Palaeozoic coral (Sinopora, Syringoporicae, Carboniferous). Histor Biol. 2014; 27(8):1098–1112.

[52]. Stolarski J, Mazur M. Nanostructure of biogenic versus abiogenic calcium carbonate crystals. Acta Palaeontol Polon. 2005; 50(4):847–865.

[53]. Cusack M, England J, Dalbeck P, Tudhope AW, Fallick AE, Allison N. Electron backscatter diffraction (EBSD) as a tool for detection of coral diagenesis. Coral Reefs. 2008; 27(4):905–911.

[54]. Mouchi V, Vonlanthen P, Verrecchia EP, Crowley QG. Multi-scale crystallographic ordering in the cold-water coral Lophelia pertusa. Sci Rep. 2017; 7(1)

[55]. Muscatine L, Goiran C, Land L, Jaubert J, Cuif J-P, Allemand D. Stable isotopes (δ13C and δ15N) of organic matrix from coral skeleton. Procs Natl Acad Sci. 2005; 102(5):1525–1530.

[56]. Gilbert PU, Porter SM, Sun C-Y, Xiao S, Gibson BM, Shenkar N, Knoll AH. Biomineralization by particle attachment in early animals. Procs Natl Acad Sci. 2019; 116:17659–17665.

[57]. Gilbert, PUPA. Photoemission spectromicroscopy for the biomineralogistBiomineralization Sourcebook, Characterization of Biominerals and Biomimetic Materials. DiMasi, E, Gower, LB, editors. CRC Press; 2014. 135–151.

[58]. DeVol RT, Metzler RA, Kabalah-Amitai L, Pokroy B, Politi Y, Gal A, Addadi L, Weiner S, Fernandez-Martinez A, Demichelis R, Gale JD, et al. Oxygen spectroscopy and polarization-dependent imaging contrast (PIC)-mapping of calcium carbonate minerals and biominerals. J Phys Chem B. 2014; 118(28):8449–57. [PubMed: 24821199]

[59]. Pokroy B, Kabalah-Amitai L, Polishchuk I, DeVol RT, Blonsky AZ, Sun C-Y, Marcus MA, Scholl A, Gilbert PUPA. Narrowly distributed crystal orientation in biomineral vaterite. Chem Mater. 2015; 27(19):6516–6523.

[60]. Gilbert PUPA, Bergmann KD, Myers CE, Marcus MA, DeVol RT, Sun C-Y, Blonsky AZ, Tamre E, Zhao J, Karan EA, Tamura N, et al. Nacre tablet thickness records formation temperature in modern and fossil shells. Earth Plan Sci Lett. 2017; 460:281–292.

[61]. De Stasio G, Capozi M, Lorusso GF, Baudat PA, Droubay TC, Perfetti P, Margaritondo G, Tonner BP. MEPHISTO: Performance tests of a novel synchrotron imaging photoelectron spectromicroscope. Rev Sci Instrum. 1998; 69(5):2062–2066.

[62]. Gránásy L, Tóth GI, Warren JA, Podmaniczky F, Tegze G, Rátkai L, Pusztai T. Phase-field modeling of crystal nucleation in undercooled liquids – A review. Progr Mat Sci. 2019

[63]. Cui X, Rohl AL, Shtukenberg A, Kahr B. Twisted aspirin crystals. J Am Chem Soc. 2013; 135(9):3395–3398. [PubMed: 23425247]

[64]. Shtukenberg AG, Punin YO, Gunn E, Kahr B. Spherulites. Chem Rev. 2012; 112(3):1805–38. [PubMed: 22103741]

[65]. De Stasio G, Frazer BH, Gilbert B, Richter KL, Valley JW. Compensation of charging in X-PEEM: a successful test on mineral inclusions in 4.4 Ga old zircon. Ultramicroscopy. 2003; 98(1):57–62. [PubMed: 14609643]

[66]. GG-Macros. 2019. http://home.physics.wisc.edu/gilbert/software.htm

[67]. Gilbert PUPA, Young A, Coppersmith SN. Measurement of c-axis angular orientation in calcite (CaCO3) nanocrystals using x-ray absorption spectroscopy. Procs Natl Acad Sci. 2011; 108:11350–11355.

[68]. DeVol RT, C-Sun Y, Marcus MA, Coppersmith SN, Myneni SCB, Gilbert PUPA. Nanoscale transforming mineral phases in fresh nacre. J Am Chem Soc. 2015; 137(41):13325–13333. [PubMed: 26403582]

[69]. Parasassi T, Sapora O, Giusti AM, De Stasio G, Ravagnan G. Alterations in erythrocyte-membrane lipids induced by low-doses of ionizing-radiation as revealed by 1,6-diphenyl-1,3,5-hexatriene fluorescence lifetime. Int J Rad Biol. 1991; 59(1):59–69. [PubMed: 1671076]

[70]. Gránásy L, Pusztai T, Börzsönyi T, Warren JA, Douglas JF. A general mechanism of polycrystalline growth. Nat Mater. 2004; 3(9):645–50. [PubMed: 15300243]

[71]. Gránásy L, Pusztai T, Tegze G, Warren JA, Douglas JF. Growth and form of spherulites. Phys Rev E. 2005; 72(1)

[72]. Wainwright SA. Studies of the mineral phase of coral skeleton. Experimental Cell Research. 1964; 34(2):213–230.

[73]. Stolarski J. Three-dimensional micro-and nanostructural characteristics of the scleractinian coral skeleton: a biocalcification proxy. Acta Palaeontologica Polonica. 2003; 48(4)

[74]. Shapiro OH, Kramarsky-Winter E, Gavish AR, Stocker R, Vardi A. A coral-on-a-chip microfluidic platform enabling live-imaging microscopy of reef-building corals. Nature communications. 2016; 7

[75]. Mouchi V, Vonlanthen P, Verrecchia EP, Crowley QG. Multi-scale crystallographic ordering in the cold-water coral Lophelia pertusa. Scientific Reports. 2017; 7(1)

[76]. Kitahara MV, Cairns SD, Stolarski J, Blair D, Miller DJ. A comprehensive phylogenetic analysis of the Scleractinia (Cnidaria, Anthozoa) based on mitochondrial CO1 sequence data. PLoS One. 2010; 5(7):e11490. [PubMed: 20628613]

[77]. Meibom A, J-Cuif P, Hillion F, Constantz BR, Juillet-Leclerc A, Dauphin Y, Watanabe T, Dunbar RB. Distribution of magnesium in coral skeleton. Geophys Res Lett. 2004; 31(23)

[78]. Raddatz J, Liebetrau V, Rüggeberg A, Hathorne E, Krabbenhöft A, Eisenhauer A, Böhm F, Vollstaedt H, Fietzke J, López Correa M, et al. Stable Sr-isotope, Sr/Ca, Mg/Ca, Li/Ca and Mg/Li ratios in the scleractinian cold-water coral Lophelia pertusa. Chem Geol. 2013:352–152. 143–152.

[79]. Rollion-Bard C, Blamart D. Possible controls on, Li, Na, and Mg incorporation into aragonite coral skeletons. Chem Geol. 2015; 396:98–111.

[80]. Finch AA, Allison N. Mg structural state in coral aragonite and implications for the paleoenvironmental proxy. Geophys Res Lett. 2008; 35(8)

[81]. Adkins JF, Boyle EA, Curry WB, Lutringer A. Stable isotopes in deep-sea corals and a new mechanism for "vital effects". Geochim Cosmochim Acta. 2003; 67(6):1129–1143.

[82]. Pokroy B, Quintana JP, Caspi EN, Berner A, Zolotoyabko E. Anisotropic lattice distortions in biogenic aragonite. Nat Mater. 2004; 3(12):900–902. [PubMed: 15543151]

[83]. Gladfeiter EH. Skeletal development in *Acropora cervicornis*: I. Patterns of calcium carbonate accretion in the axial corallite. Coral Reefs. 1982; 1(1):45–51.

[84]. Le Tissier MDAA. Diurnal patterns of skeleton formation in *Pocillopora damicornis* (Linnaeus). Coral Reefs. 1988; 7(2):81–88.

[85]. Gilis M, Meibom A, Domart-Coulon I, Grauby O, Stolarski J, Baronnet A. Biomineralization in newly settled recruits of the scleractinian coral Pocillopora damicornis. J Morphol. 2014; 275(12):1349–65. [PubMed: 24966116]

[86]. Hedaka, M. Fusiform and needle-shaped crystals found on the skeleton of a coralGalaxea fascicularis. Springer; Japan, Tokyo: 1991. 139–143.

[87]. Clode PL, Marshall AT. Skeletal microstructure of *Galaxea fascicularis* exsert septa: a high-resolution SEM study. Biol Bull. 2003; 204(2):146–154. [PubMed: 12700145]

[88]. Raz-Bahat M, Erez J, Rinkevich B. In vivo light-microscopic documentation for primary calcification processes in the hermatypic coral Stylophora pistillata. Cell Tissue Res. 2006; 325(2):361–368. [PubMed: 16568301]

[89]. Cuif J, Dauphin Y, Denis A, Gautret P, Marin F. The organo-mineral structure of coral skeletons: a potential source of new criteria for Scleractinian taxonomy. Bull Inst Oceanogr Monaco-Numero Special-. 1996:359–368.

[90]. Stolarski J, Bosellini FR, Wallace CC, Gothmann AM, Mazur M, Domart-Coulon I, Gutner-Hoch E, Neuser RD, Levy O, Shemesh A, Meibom A. A unique coral biomineralization pattern has resisted 40 million years of major ocean chemistry change. Sci Rep. 2016; 6

[91]. McHale J, Auroux A, Perrotta A, Navrotsky A. Surface energies and thermodynamic phase stability in nanocrystalline aluminas. Science. 1997; 277(5327):788–791.

[92]. Yang L, Killian CE, Kunz M, Tamura N, Gilbert PUPA. Biomineral nanoparticles are space-filling. RSC-Nanoscale. 2011; 3:603–609.

[93]. Podmaniczky F, Tóth GI, Tegze G, Gránásy L. Hydrodynamic theory of freezing: nucleation and polycrystalline growth. Phys Rev E. 2017; 95(5)

[94]. Mass T, Giuffre AJ, Sun C-Y, Stifler CA, Frazier MJ, Neder M, Tamura N, Stan CV, Marcus MA, Gilbert PUPA. Amorphous calcium carbonate particles form coral skeletons. Procs Natl Acad Sci. 2017; 114(37):E7670–E7678.

[95]. Jiang Y, Gong H, Grzywa M, Volkmer D, Gower L, Cölfen H. Microdomain transformations in mosaic mesocrystal thin films. Adv Funct Mater. 2013; 23(12):1547–1555.

[96]. Sevilgen DS, Venn AA, Hu MY, Tambutté E, de Beer D, Planas-Bielsa V, Tambutté S. Full in vivo characterization of carbonate chemistry at the site of calcification in corals. Sci Adv. 2019; 5(1):eaau7447. [PubMed: 30746460]

[97]. Voorhees PW. The theory of Ostwald ripening. J Stat Phys. 1985; 38(1–2):231–252.

[98]. Ratke L, Voorhees PW. Growth and coarsening: Ostwald ripening in material processing. Springer Science & Business Media. 2013

[99]. Stoldt C, Jenks CJ, Thiel PA, Cadilhe A, Evans JW. Smoluchowski ripening of Ag islands on Ag (100). J Chem Phys. 1999; 111(11):5157–5166.

[100]. Gerber T, Knudsen J, Feibelman PJ, Granas E, Stratmann P, Schulte K, Andersen JN, Michely T. CO-induced Smoluchowski ripening of Pt cluster arrays on the graphene/Ir (111) moiré. ACS Nano. 2013; 7(3):2020–2031. [PubMed: 23379255]

[101]. Bayerlein B, Zaslansky P, Dauphin Y, Rack A, Fratzl P, Zlotnikov I. Self-similar mesostructure evolution of the growing mollusc shell reminiscent of thermodynamically driven grain growth. Nat Mater. 2014; 13(12):1102–7. [PubMed: 25326825]

[102]. Reed-Hill, RE, Abbaschian, R. Physical metallurgy principles. 3rd ed. PWS-Kent; Boston, MA: 1992.

[103]. Schoeppler V, Gránásy L, Reich E, Poulsen N, de Kloe R, Cook P, Rack A, Pusztai T, Zlotnikov I. Biomineralization as a paradigm of directional solidification: a physical model for molluscan shell ultrastructural morphogenesis. Adv Mater. 2018:e1803855. [PubMed: 30239045]

[104]. Schoeppler V, Lemanis R, Reich E, Pusztai T, Gránásy L, Zlotnikov I. Crystal growth kinetics as an architectural constraint on the evolution of molluscan shells. Procs Natl Acad Sci. 2019; 116(41):20388–20397.

[105]. Granasy L, Pusztai T, Tegze G, Warren JA, Douglas JF. Growth and form of spherulites. Phys Rev E. 2005; 72(1):011605.

[106]. Puverel S, Tambutte E, Pereira-Mouries L, Zoccola D, Allemand D, Tambutte S. Soluble organic matrix of two Scleractinian corals: partial and comparative analysis. Comp Biochem Physiol B Biochem Mol Biol. 2005; 141(4):480–7. [PubMed: 15982916]

[107]. Ogilvie MM. Microscopic and Systematic Study of Madreporarian Types of Corals, Phil Trans R Soc London. Series B, Containing Papers of a Biological Character. 1896; 187:83–345.

[108]. Metzler RA, Zhou D, Abrecht M, J-Chiou W, Guo J, Ariosa D, Coppersmith SN, Gilbert PUPA. Polarization-dependent imaging contrast in abalone shells. Phys Rev B. 2008; 77

[109]. Olson IC, Metzler RA, Tamura N, Kunz M, Killian CE, Gilbert PUPA. Crystal lattice tilting in prismatic calcite. J Struct Biol. 2013; 183:180–190. [PubMed: 23806677]

[110]. Zhong C, Chu CC. On the origin of amorphous cores in biomimetic CaCO3 spherulites: new insights into spherulitic crystallization. Cryst Growth Des. 2010; 10(12):5043–5049.

[111]. Keller A. The spherulitic structure of crystalline polymers. Part II. The problem of molecular orientation in polymer spherulites. J Polym Sci. 1955; 17(85):351–364.

[112]. Ergoz E, Fatou J, Mandelkern L. Molecular weight dependence of the crystallization kinetics of linear polyethylene. I Experimental results, Macromol. 1972; 5(2):147–157.

[113]. Mandelkern L. The relation between structure and properties of crystalline polymers. Polym J. 1985; 17(1):337–350.

[114]. Jenkins M, Harrison K. The effect of molecular weight on the crystallization kinetics of polycaprolactone. Polym Adv Technol. 2006; 17(6):474–478.

[115]. Strobl G, Hagedorn W. Raman spectroscopic method for determining the crystallinity of polyethylene. J Polym Sci: Polym Phys Ed. 1978; 16(7):1181–1193.

[116]. Glotin M, Mandelkern L. A Raman spectroscopic study of the morphological structure of the polyethylenes. Coll Polym Sci. 1982; 260(2):182–192.

[117]. Taylor LS, Zografi G. The quantitative analysis of crystallinity using FT-Raman spectroscopy. Pharm Res. 1998; 15(5):755–761. [PubMed: 9619786]

[118]. Yang Y, Chen M, Li H, Li H. The degree of crystallinity exhibiting a spatial distribution in polymer films. Eur Polym J. 2018; 107:303–307.

[119]. Shtukenberg AG, Hu CT, Zhu Q, Schmidt MU, Xu W, Tan M, Kahr B. The third ambient aspirin polymorph. Crystal Growth & Design. 2017; 17(6):3562–3566.

[120]. Cui X, Rohl AL, Shtukenberg A, Kahr B. Twisted aspirin crystals. Journal of the American Chemical Society. 2013; 135(9):3395–3398. [PubMed: 23425247]

[121]. Palmer BA, Yallapragada VJ, Schiffmann N, Wormser EM, Elad N, Aflalo ED, Sagi A, Weiner S, Addadi L, Oron D. A highly reflective biogenic photonic material from core–shell birefringent nanoparticles. Nature Nanotechnology. 2020:1–7.

[122]. Yallapragada VJ, Oron D. Optical properties of spherulite opals. Optics letters. 2019; 44(23):5860–5863. [PubMed: 31774798]

[123]. Miao B, Wood DN, Bian W, Fang K, Fan MH. Structure and growth of platelets in graphite spherulites in cast iron. Journal of materials science. 1994; 29(1):255–261.

[124]. Fernandes VA, Müller AJ, Sandoval AJ. Thermal, structural and rheological characteristics of dark chocolate with different compositions. Journal of Food Engineering. 2013; 116(1):97–108.

Europe PMC Funders Author Manuscripts

Europe PMC Funders Author Manuscripts

Statement of Significance

Understanding the fundamental mechanisms of spherulite nucleation and growth has broad ranging applications in the fields of metallurgy, food science, and pharmaceutical production. Using the skeletons of reef-building corals as a model system for investigating these processes, we propose a new spherulite growth mechanism that can not only explain the micro-structural diversity observed in distantly related coral species, but may point to a universal growth mechanism in a wide range of biologically and technologically relevant spherulitic materials systems.

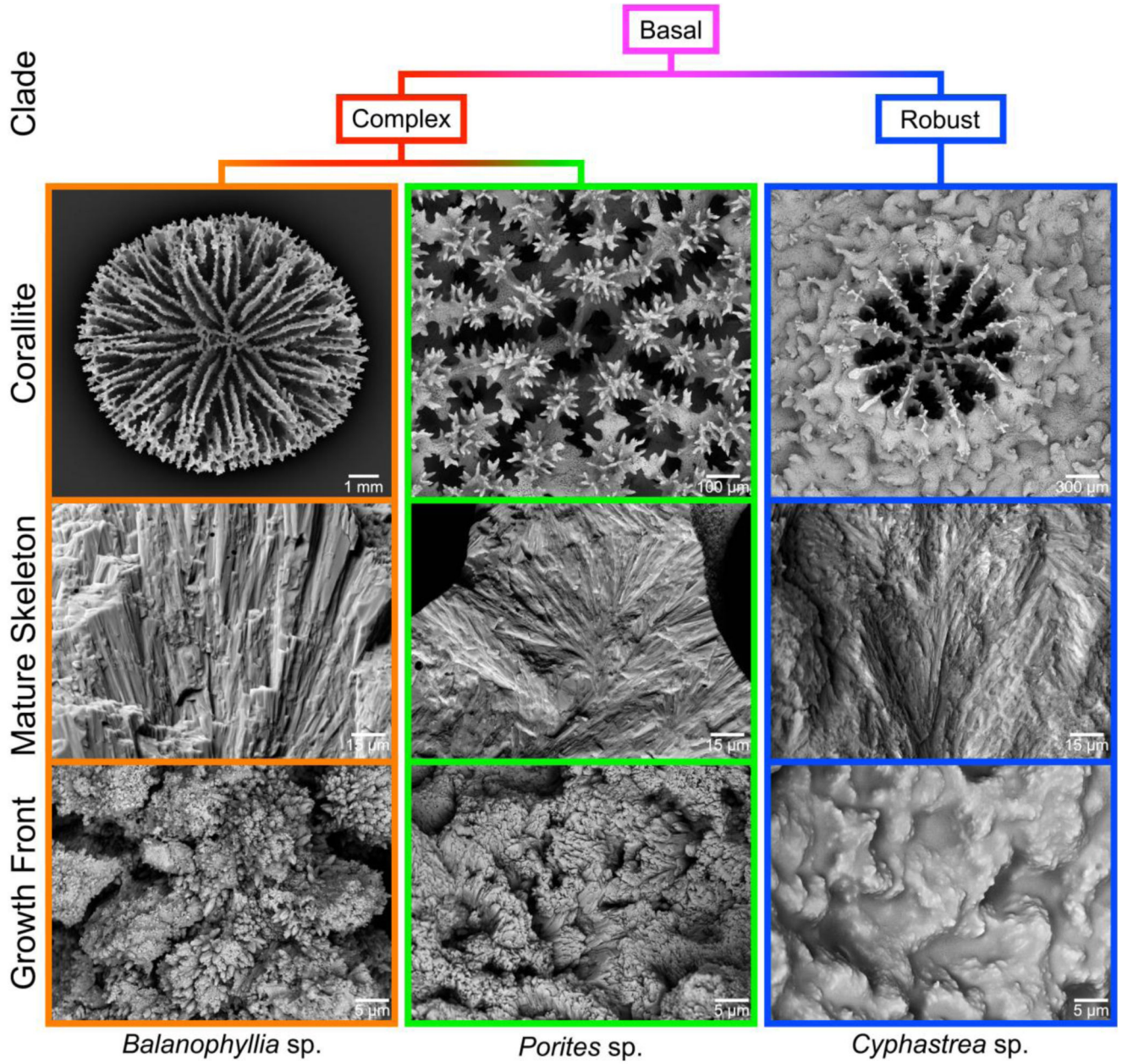

Figure 1.

Scanning electron microscopy (SEM) images of corallites from three distantly related coral genera: *Balanophyllia*, *Porites*, and *Cyphastrea* (top row). The bulk mature skeleton is always spherulitic (middle row), but the fine-scale morphology at the growth front varies widely across corals (bottom row).

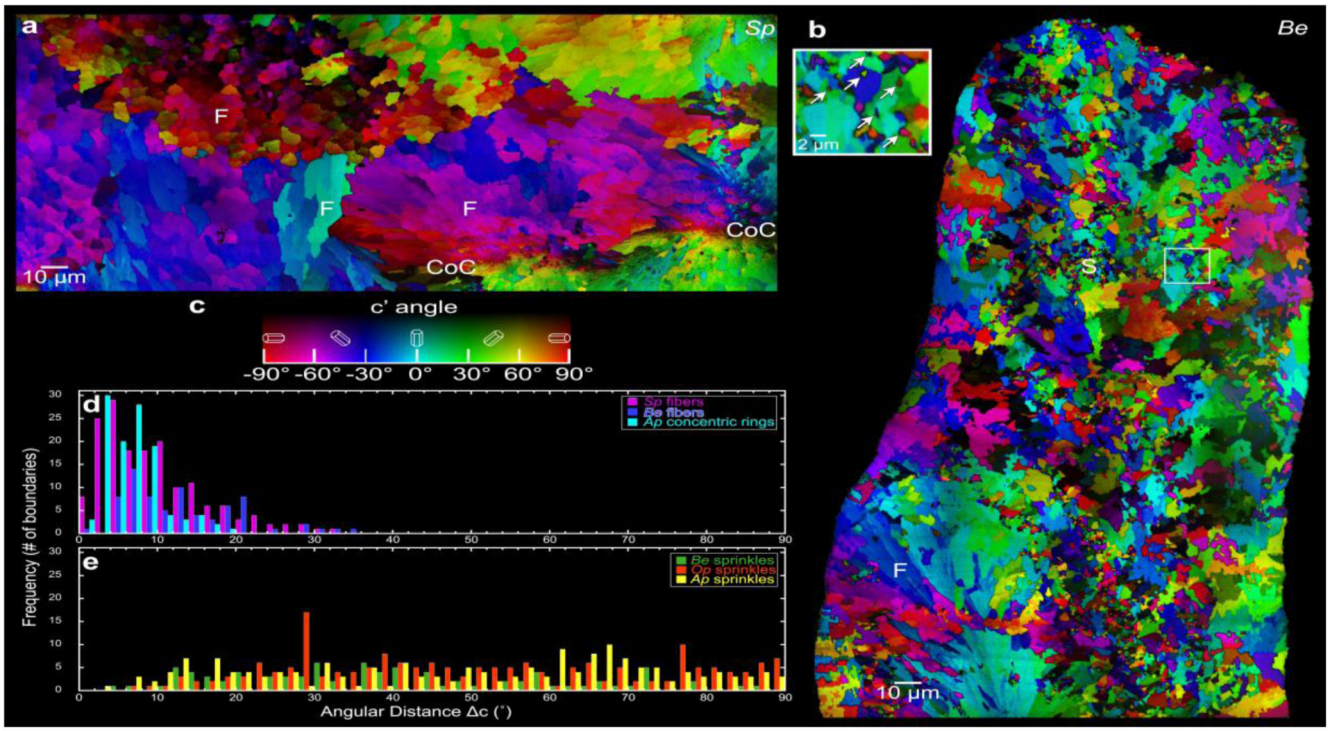

Figure 2.

Merged PIC maps of (a) *Stylophora pistillata* (*Sp*) and (b) *Balanophyllia europaea* (*Be*) coral skeletons. (c) Color bar for PIC maps in (a) and (b). Centers of calcification (CoC) extend along a non-straight line between the two CoC labels in *Sp*. No CoCs are visible in this particular *Be* region. Notice the acicular crystal fibers (F) characteristic of spherulites, changing color and thus orientation only slightly across grain boundaries, and sprinkles (S), which are smaller crystals changing color abruptly across boundaries. Sprinkles are found in the mature (bulk) skeletons of *Be*, but not in *Sp*, whereas spherulitic crystals appear in both skeletons. Inset in (b) shows a higher magnification PIC map of the sprinkles, which are indicated by the arrows and are interspersed with spherulitic crystals. (d) Distributions of angular distances between the *c-ax*es of adjacent crystals in spherulitic crystals in *Sp* and *Be* skeletons, and in concentric rings of *Acropora pharaonis* (*Ap*) skeletons (Fig. 7). (e) Identically measured distributions in the sprinkles of *Be*, *Oculina patagonica* (*Op*), and *Ap* skeletons. Notice that in spherulitic crystals, the angular distances are always within 35°, whereas in sprinkles, they are random (0–90°). Details of the angular distance measurement and the ROI selections are described in the Experimental Methods and Figure S4.

Europe PMC Funders Author Manuscripts

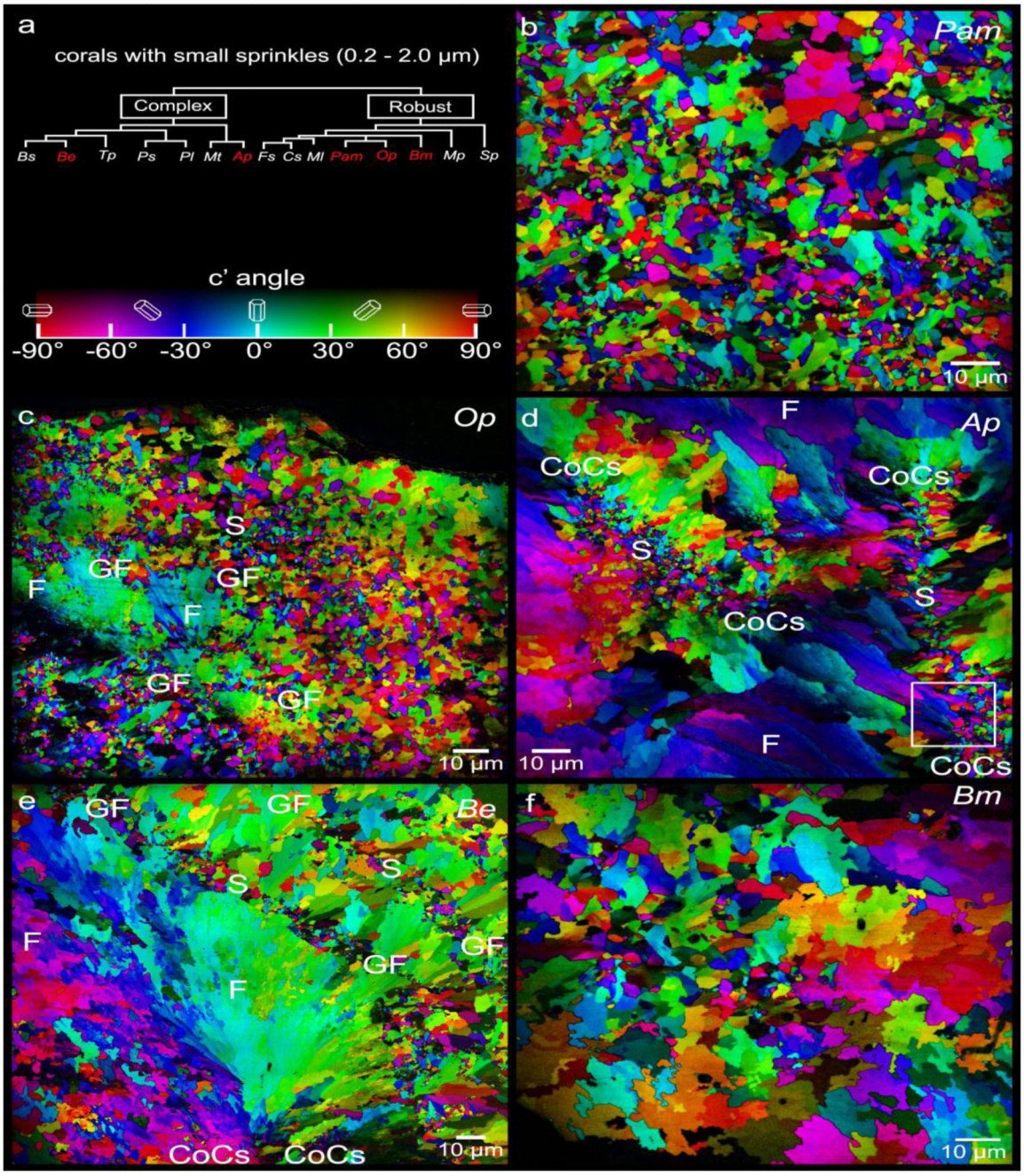

Figure 3.

PIC maps of the 5 coral species that exhibit abundant small (0.2-2µm) sprinkles across their skeletons. These are *Phyllangia americana mouchezii (Pam), Oculina patagonica (Op), Acropora pharaonis (Ap), Balanophyllia europaea* (*Be*), and *Blastomussa merleti (Bm)*. Sprinkles (S) appear as randomly colored and oriented crystals smaller than fiber (F) crystals. In *Ap* they are localized in centers of calcification (CoCs, between pairs of CoC labels), in *Op* and *Be* at the surfaces of fiber bundles, which during coral skeleton growth

were the growth fronts (GF, between pairs of GF labels). In *Pam* and *Bm* sprinkles appear everywhere interspersed with fibers. The box in d is magnified in Figure 6d.

Europe PMC Funders Author Manuscripts

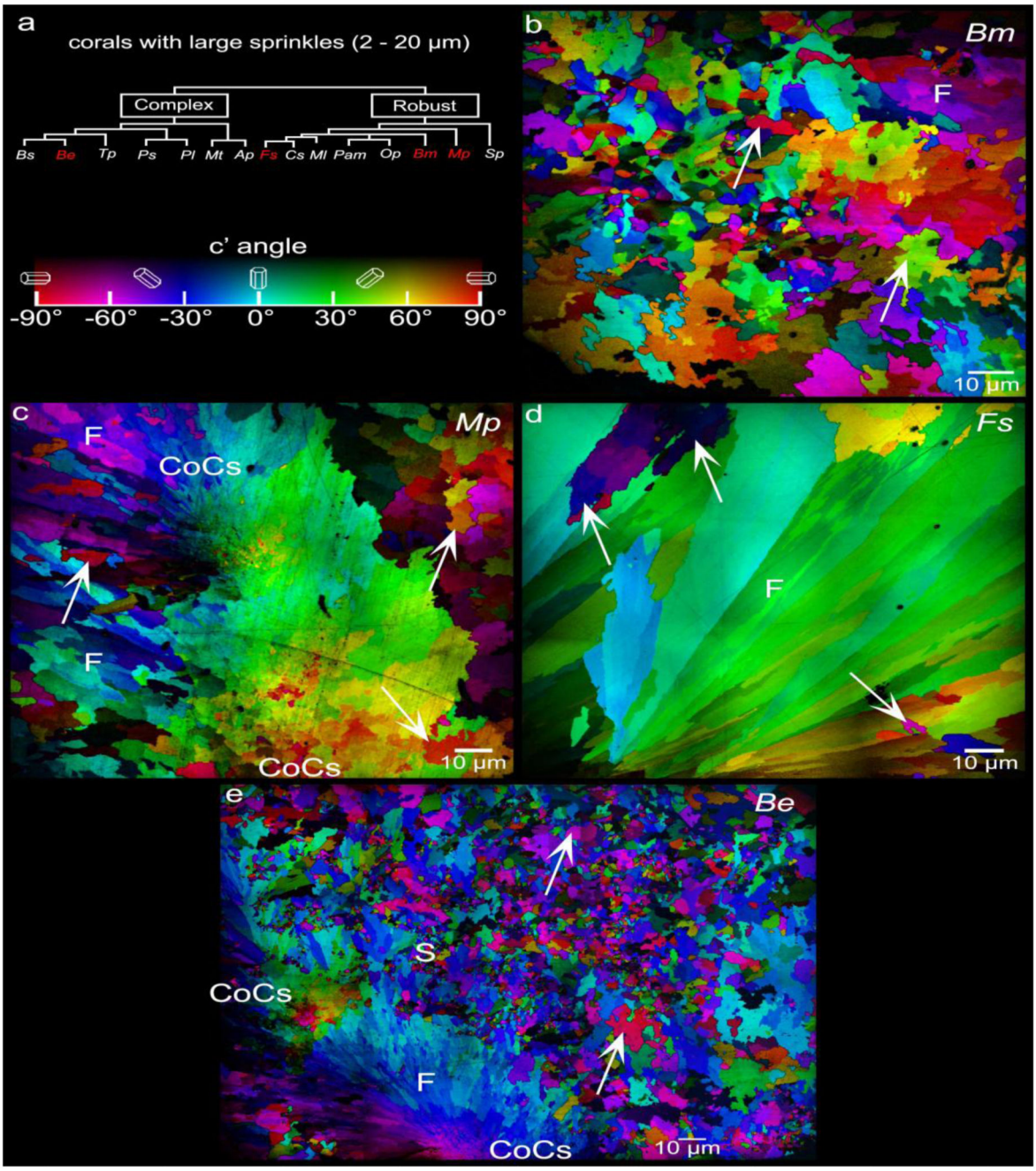

Figure 4.

PIC maps of the 4 coral species that exhibit large (2-20μm) sprinkles across their skeletons. These are *Blastomussa merleti (Bm), Madracis pharensis (Mp), Favia* sp. *(Fs)*, and -*Balanophyllia europaea* (*Be*). Arrows indicate a few large sprinkles, but many more are visible. Large sprinkles are distinct from fibers (F) not by size but by crystal orientations: they form >35° angles with their neighboring crystals, whereas fiber crystals only form small angles (<35°) with respect adjacent fibers in the same bundle. Nanoparticulate crystals (between pairs of CoC labels) are visible in the CoCs of *Mp* and *Be.* Nanocrystals in the

CoCs are not randomly oriented, but rather oriented similarly to their neighboring crystals. CoCs, therefore, cannot be sprinkles.

Europe PMC Funders Author Manuscripts

Europe PMC Funders Author Manuscripts

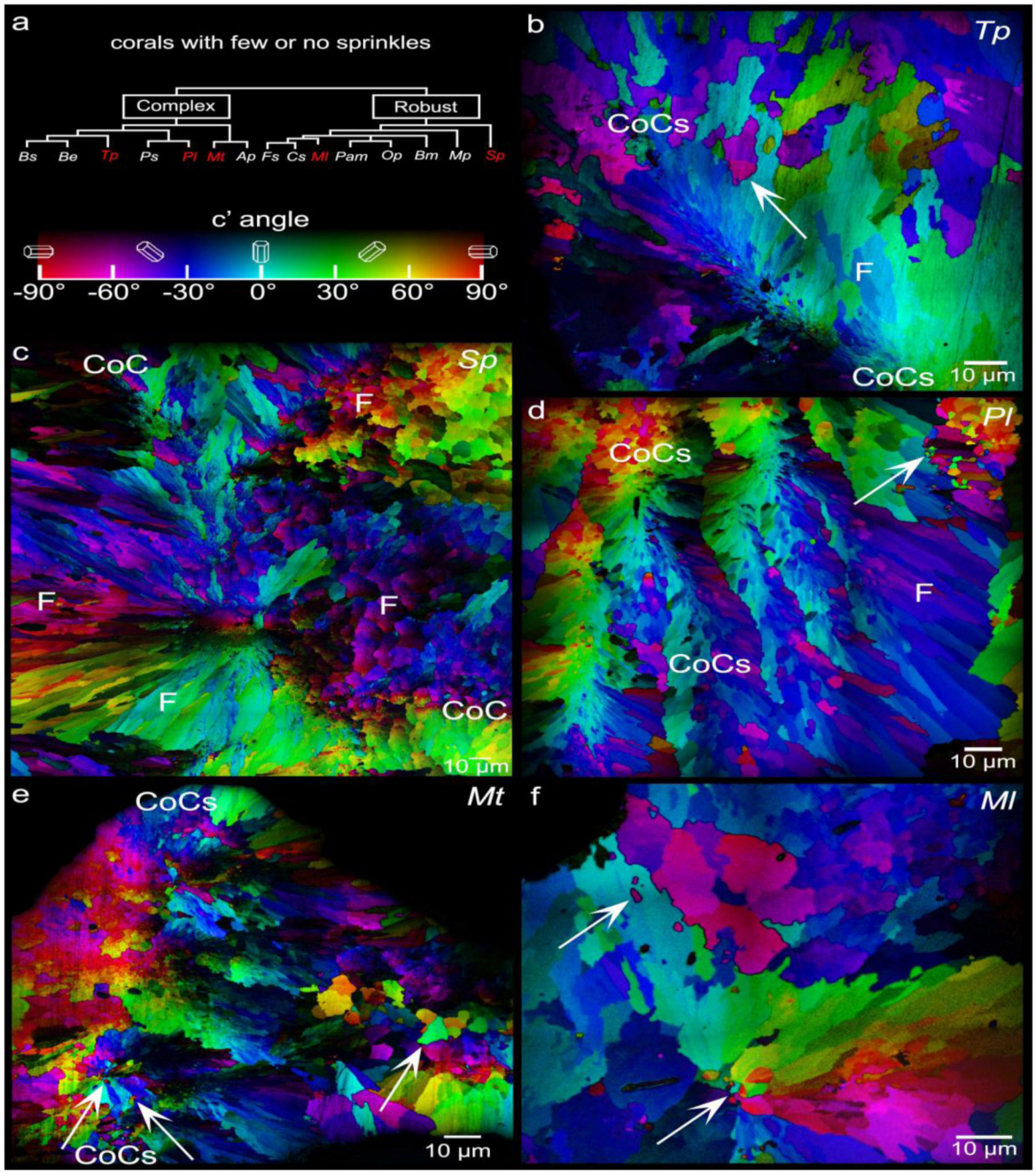

Figure 5.

PIC maps of the 5 coral species that exhibit few or no sprinkles. These are *Turbinaria peltata (Tp), Stylophora pistillata (Sp), Porites lutea (Pl), Montipora turgescens (Mt)*, and *Micromussa lordhowensis (Ml)*. Again centers of calcification (CoCs, between pairs of CoC labels) are distinguishable by their nanoparticulate appearance along a straight line in *Tp*, a long tortuous line in *Sp*, four parallel lines in *Pl* only one of which is between CoC labels, and in *Mt*. As in Figure 4, none of these CoCs exhibit any sprinkles. Arrows indicate the

very few visible sprinkles. These are so few that they could belong to out-of-plane bundles of fibers, thus these 5 species are described as non-sprinkle retaining.

Europe PMC Funders Author Manuscripts

Europe PMC Funders Author Manuscripts

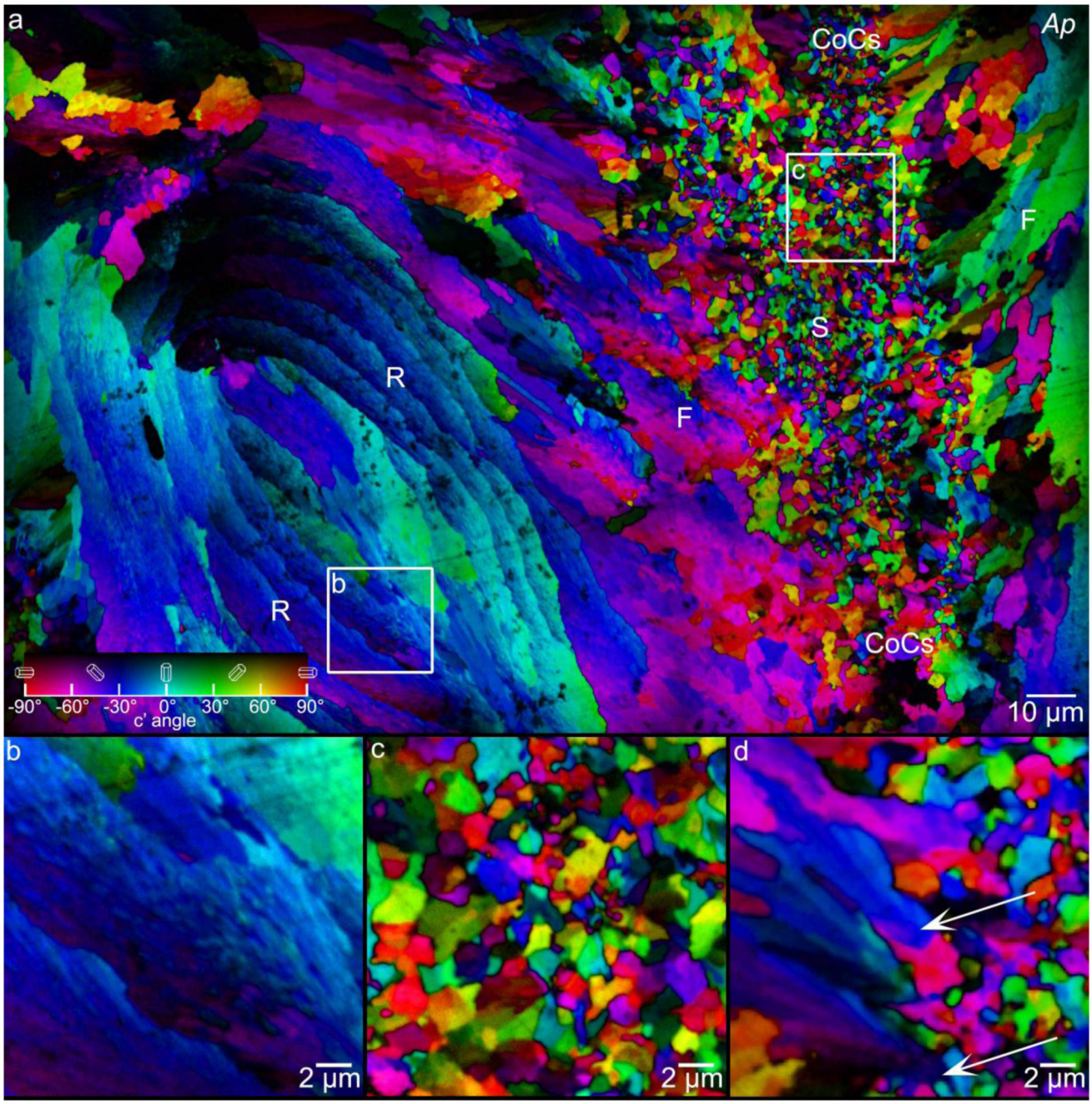

Figure 6.

a: PIC map of *Acropora pharaonis* (*Ap)* coral skeleton, showing sprinkles (S) concentrated at the CoCs (between pairs of CoC labels), spherulitic crystal fibers (F) fanning out from the CoCs, and concentric rings (R), which consist of finer spherulitic fiber crystals. Boxes b, c indicate the areas magnified in panels b, c. b: Magnified concentric rings, showing that these are made of nearly co-oriented acicular crystals. c: Magnified sprinkles from CoCs. d: Sprinkles at the boundary of CoCs and fiber crystals, magnified from the box area in Figure 3d. Arrows indicate two blue sprinkles that expand radially into -30° oriented fibers. Red

and green sprinkles do not grow as they run into other crystals. In panels a and d pixels are 60 nm, in b and c they are 20 nm.

Europe PMC Funders Author Manuscripts

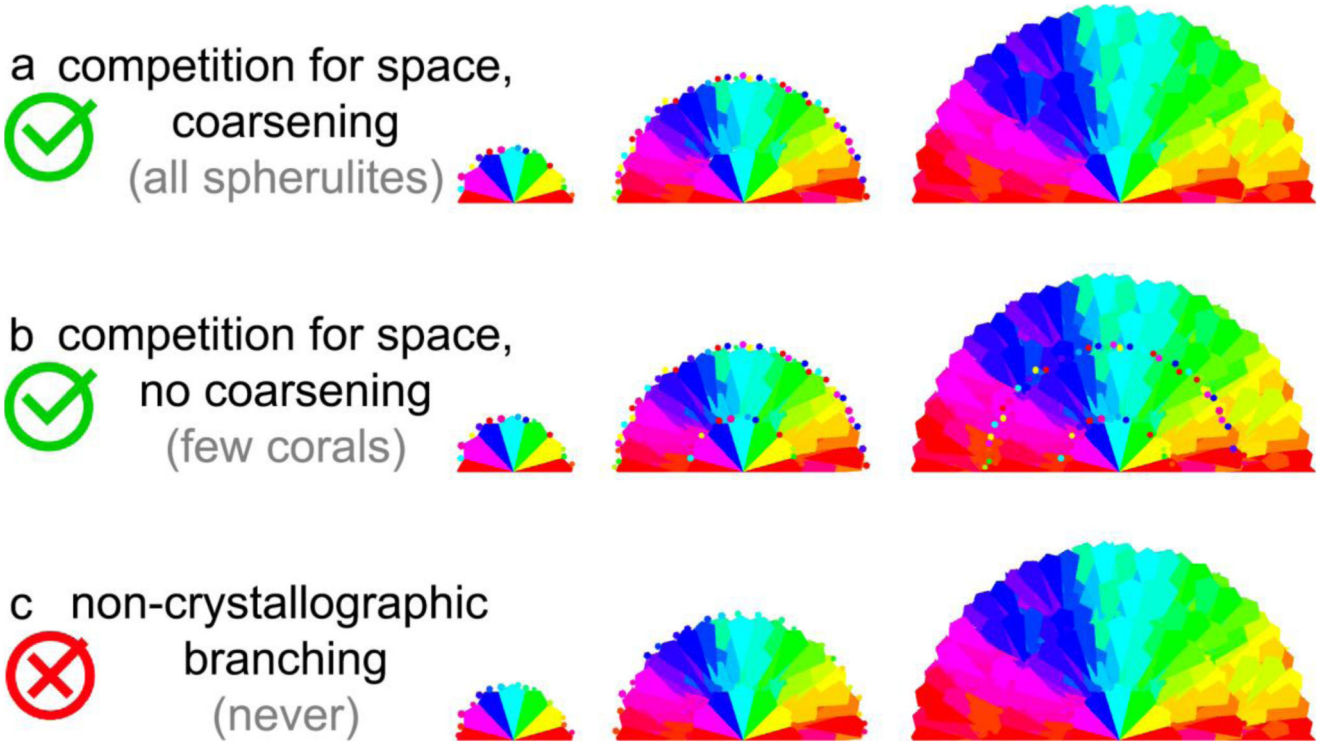

Figure 7.

Schematic of spherulite growth mechanisms. All cases a, b, c share growth front nucleation (GFN), and, in the final spherulite, radial crystals oriented and thus colored similarly to their neighboring crystals. a. This is the spherulite formation mechanism proposed here: All newly nucleating crystals have random orientations (small hexagons with diverse colors, termed sprinkles), and because of competition for space they grow only if they are radially oriented. Coarsening makes larger crystals grow at the expense of smaller crystals, thus resulting in sprinkle-free spherulites. b. In a subset of coral skeletons the sprinkles are retained, because of incomplete or absent coarsening. These are the exceptional cases suggesting the formation mechanism for all spherulites, potentially. c. All newly nucleating crystals have orientation similar but not identical to the mother crystal. This previous assumption was termed non-crystallographic branching, and is ruled out by the alternative growth mechanism in a, inspired by coral skeletons.

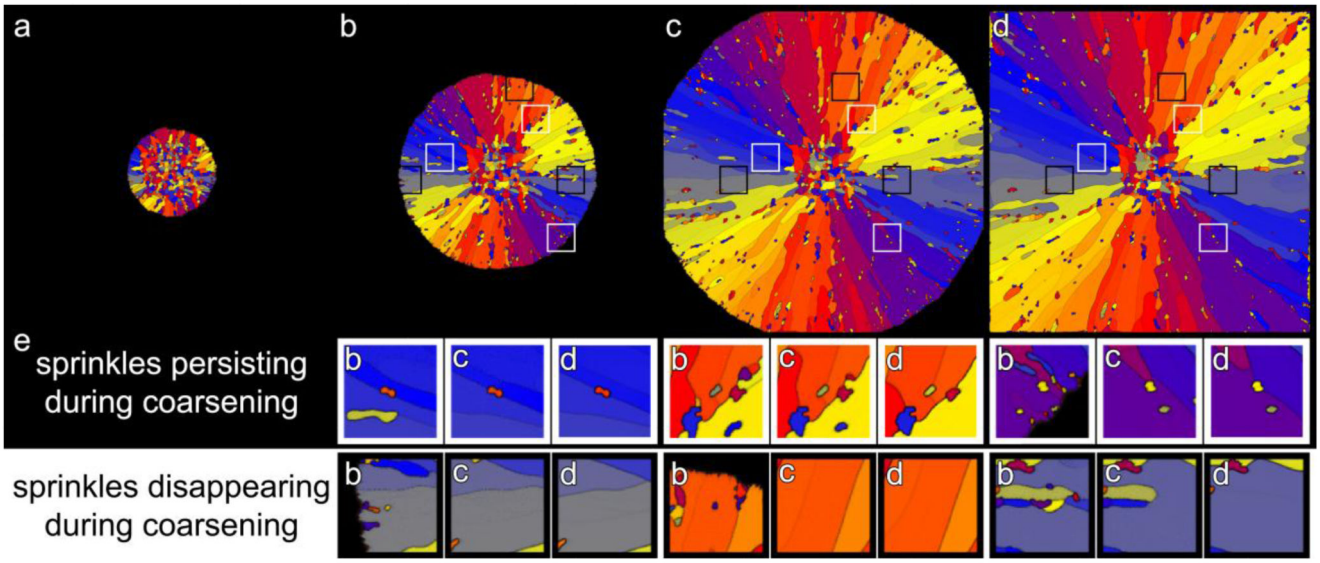

Figure 8.

Phase-field simulation of spherulitic growth from sprinkles. a-d: Time series of the spherulite growth from sprinkles, showing frames 6, 21, 41, 60 of the simulation. a: An early frame in which sprinkles are formed, with random orientation, by nucleation from a solution with high supersaturation. b,c,d: Elongated crystal fibers grow from each sprinkle. Radially oriented crystals continue to elongate, whereas transversally oriented ones abut one another and stop growing. This growth process ultimately results in radially oriented crystals with slight misorientation across grain boundaries, that is, spherulitic growth. Notice that sprinkles nucleate at the liquid-solid interface during GFN. Three white boxes and three black boxes are positioned in identical locations in b, c, d, and are centered around a sprinkle that persists or disappears, respectively. e: Magnified images of the details boxed in b,c,d, panels shown as a function of time in each b,c,d triplet. At the center of the white boxes the sprinkle persists while other sprinkles disappear. In the black boxes at the bottom, almost all sprinkles disappear due to coarsening, which may occur by Ostwald or Smoluchowski ripening, if the system is locally liquid or solid, respectively. Locally slow, incomplete, or gradual solidification enables sprinkle shrinking or rotation.

Europe PMC Funders Author Manuscripts

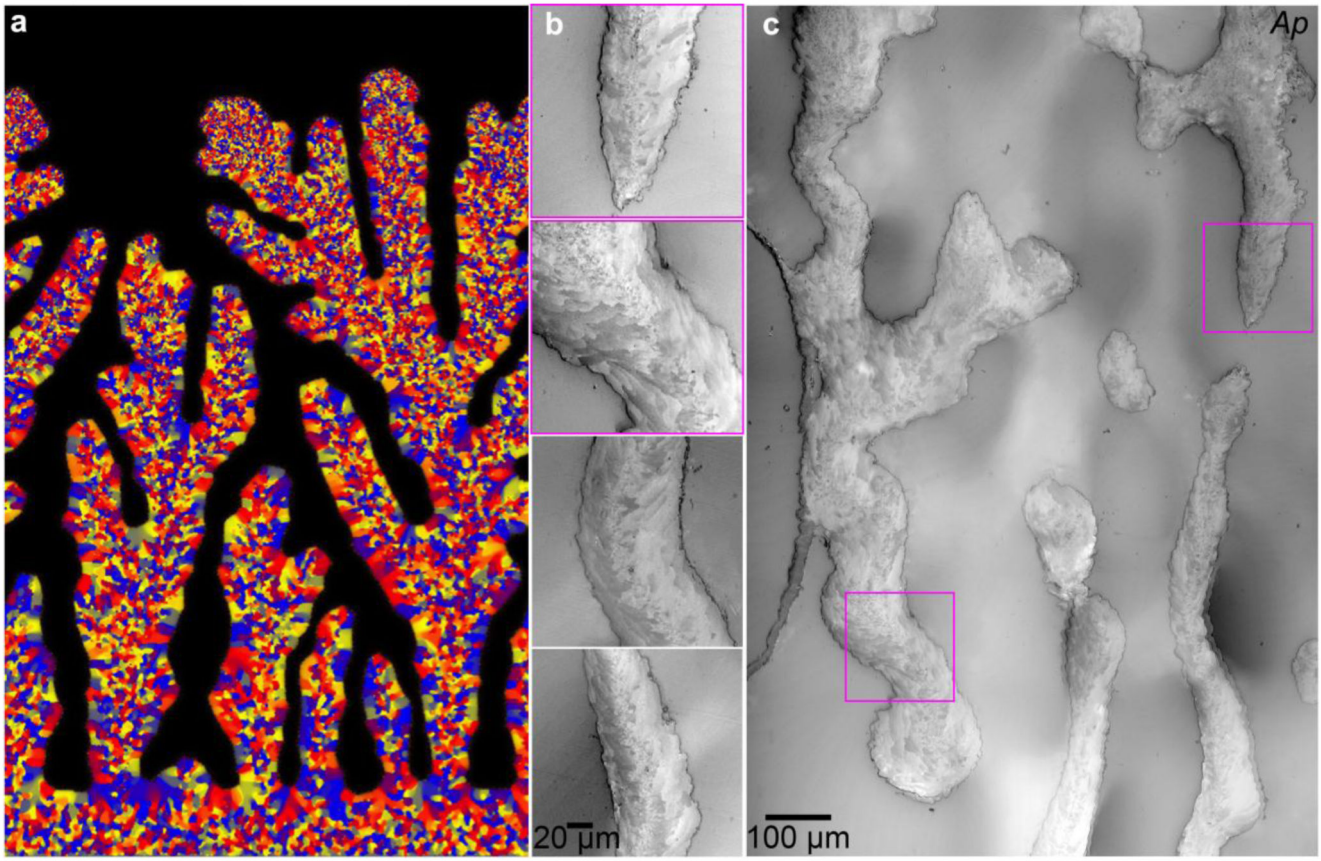

Figure 9.

Phase-field simulation of coral skeleton grown from sprinkles. a: Simulated orientation map in which sprinkles form at the tip of each branch, termed nubbin, and become the core of each branch, where they persist. Much larger crystals form on the branch sides, which are similar to the large sprinkles (2-20 μm). b,c: PLM images from two distinct *Acropora pharaonis* (*Ap*) coral skeletons. The top two panels in b are cropped and magnified from the areas indicated by magenta boxes in c, the bottom two panels are from a different *Ap* skeleton. The overall morphology in c, and the details in b, including sprinkles at the center, and fibers at the sides of each nubbin, are all similar to the simulated ones in a, except that the fibers in b and c are elongated and thinner than the side crystals in a.

Table 1

Summary of all coral species studied here, and the crystal structures observed in their mature skeletons.

spherulitic fibers and CoCs				*Stylophora pistillata (Sp)*	Robust	Branching	Red Sea	sub-tropical
				Turbinaria peltata (Tp)	Complex	Table-like	Indo-Pacific	tropical
				Porites lutea (Pl)	Complex	Massive	Red Sea	sub-tropical
				Montipora turgescens (Mt)	Complex	Encrusting	Indo-Pacific	tropical
				Micromussa lordhowensis (Ml)	Robust	Massive	Indo-Pacific	tropical
	small sprinkles (0.2-2 μm)			*Phyllangia americana mouchezii (Pam)*	Robust	Encrusting	Mediterranean Sea	temperate
				Oculina patagonica (Op)	Robust	Encrusting	Mediterranean Sea	temperate
			concentric rings	*Acropora pharaonis (Ap)*	Complex	Branching	Red Sea	sub-tropical
		large sprinkles (2-20 μm)		*Blastomussa merleti (Bm)*	Robust	Massive	Indo-Pacific	tropical
				Balanophyllia europaea (Be)	Complex	Solitary	Mediterranean Sea	temperate
				Madracis pharensis (Mp)	Robust	Encrusting	Mediterranean Sea	temperate
				Favia sp. *(Fs)*	Robust	Massive	Red Sea	sub-tropical

Europe PMC Funders Author Manuscripts

Table 2

Specific surface area data measured by Brunauer-Emmett-Teller (BET) method Coral skeletons measured here by the are as space-filling as single crystals of geologic aragonite. The BET results are typical of biogenic minerals, similar to those previously published for sea urchin spines, spicules, and teeth [1], and very different from those usually measured for aggregates of nanoparticles, which are typically in the 200-300 m^2/g range and thus highly porous [2].

sample ID	specific surface area (m^2/g) 1st measurement	specific surface area (m^2/g) 2nd measurement	average
Sp coral skeleton	3.78	3.53	3.53±0.18
Be coral skeleton	4.64	3.91	4.28±0.52
Geologic aragonite	1.67	1.73	1.70±0.04